Ship Shock Trial Simulation of USS Winston S. Churchill (DDG 81): Modeling and Simulation Strategy and Surrounding Fluid Volume Effects

Young S. Shin and Nathan A. Schneider
Department of Mechanical Engineering
Naval Postgraduate School
Monterey, California 93943
(831) 656-2568, yshin@nps.navy.mil

During World War II many surface combatants were damaged or severely crippled by close-proximity underwater explosions from ordnance that had actually missed their target. Since this time all new classes of combatants have been required to conduct shock trial tests on the lead ship of the class in order to test the survivability of mission essential equipment in a severe shock environment. While these tests are extremely important in determining the vulnerabilities of a surface ship, they require an extensive amount of preparation, man-hours, and money. Furthermore, these tests present an obvious danger to the crew on board, the ship itself, and any marine life in the vicinity. Creating a virtual shock environment by use of a computer to model the ship structure and the surrounding fluid presents a valuable design tool and an attractive alternative to these tests. The research work shown in this paper investigated the accuracy of shock simulation using the shock trials conducted on USS WINSTON S. CHURCHILL (DDG 81) in 2001. All three explosions DDG 81 was subjected to are simulated and the resulting predictions compared with actual shock trial data. The ship shock modeling and simulation strategy is discussed and the effects of fluid volume size, mesh density, mesh quality are also investigated.

INTRODUCTION

In World War II, the U.S. Navy experienced the highly destructive effects of near proximity underwater explosions (UNDEX) from mines and torpedoes. Many combatants with the latest in combat technology for the time were rendered helpless due to inadequate shock proofing of the ship systems. Since this time, extensive work has gone into the research and study of the effects of UNDEX. A major goal in the design of modern combatant ships has been to eliminate or at least reduce damage caused by UNDEX.

Guidelines and specifications have been developed for the shock testing and hardening of shipboard equipment and systems. NAVSEA 0908-LP-000-3010A [1] and MIL-S-901D [2] set forth much of this guidance. As directed by OPNAVINST 9072.2 [3], the complete ship system is tested by performing what are called underwater shock trials. These shock trials attempt to test the ship under "near combat conditions" by igniting a large size of explosive in underwater at varying standoff distances from the ship. The effect of the shocks to ship systems is observed and the response of the ship is monitored and recorded for each shot. The lead ship of each class, or a ship substantially deviating from other ships of the same class, is required to undergo these trials in order to correct any deficiencies on that ship as well as the follow on ships of the class.

These shock trials, while beneficial in determining the wartime survivability of surface ships, require years of planning and preparation and are extremely expensive. In the Aegis Destroyer program alone, over 30 million dollars were spent for the shock trials conducted on USS JOHN PAUL JONES (DDG 53) in 1994 and another 20 million dollars for the shock trials conducted on USS WINSTON S. CHURCHILL (DDG 81) in 2001. In addition, these tests present an obvious danger to the crew onboard, the ship itself, and any marine life in the vicinity of the test. Due to this inherent safety risk, shock trials do not test up to the ship's design limits or even the true combat

shock environment. This has raised the question as to whether or not the information gleaned from doing the tests is worth the high cost of conducting them [4].

Advances in the capabilities of computers in the last few decades have allowed many events to be tested in a virtual world. This has allowed engineers not only to save millions of dollars, but it has also allowed for faster advancements in design. Creating a virtual UNDEX environment for ship system underwater shock testing presents an extremely useful design tool and an attractive alternative to future shock trials. This would save the Navy millions of dollars while at the same time not harm our sailors or the environment.

To obtain accurate results from a simulation, the structural finite element model must be extremely detailed. Additionally, the surrounding acoustic medium must be coupled with the wetted surface of the structural model almost perfectly. The resulting coupled fluid and structural model necessary for an accurate simulation is enormous computationally. The UNDEX environment is very complex, made up of an initial "kick" from the incident shock wave followed by the effects of cavitation, bubble pulse, and structural whipping [4,5]. While the computational time step must be very small, on the order of microseconds, the entire UNDEX ship response lasts on the order of seconds. Because shock simulations are virtual in nature, they can be conducted at or beyond design limits, providing more useful design information than that which is gained by conducting real world shock trials

This paper investigates the feasibility of creating a virtual UNDEX environment to model the response of a surface ship exposed to an underwater shock. This is accomplished using the shock trial data from the shock trial conducted on USS WINSTON S. CHURCHILL (DDG 81) in June of 2001. DDG 81 was subjected to three different underwater explosions during these trials, each explosion having a different geometry. Comparisons between the simulated response predictions and the actual measured response are made for all three shots. The effects of charge location in relation to the ship, size of the fluid mesh, fluid mesh density, and the quality of the fluid mesh are investigated. By creating an easily modified fluid mesh model, a wide range of shot and ship loading conditions can be simulated. This creates unlimited potential for future UNDEX simulation research. The modifiability of the fluid models investigated in this paper and the modeling techniques that permit this easy modification are discussed. Also, the ship shock modeling and simulation strategy is discussed

These underwater shock simulations were conducted using the most accurate and state of the art finite element ship model to date. The fluid volume models were generated using the TrueGrid finite element mesh generator program [6]. The simulation processing was conducted using the LS-DYNA/USA (Underwater Shock Analysis) coupled computer code [7,8].

FINITE ELEMENT MODEL OF DDG 81 SHIP

A finite element model (FEM) of USS WINSTON S. CHURCHILL (DDG 81) built by Gibbs & Cox, Inc [8] was used for the research summarized in this paper. This model, shown in Figure 1, is a modification of the USS JOHN PAUL JONES (DDG 53) model used in the UNDEX simulations conducted at the Naval Postgraduate School (NPS) from 1998 to 2000 [10-13].

DDG 81 is a Flight IIA Arleigh Burke Class destroyer having significant modifications from prior destroyers in the class. The major structural modifications include:

- The addition of dual helicopter hangars
- Six additional vertical launch system (VLS) cells, three forward and three aft
- Installation of a 5"/62 caliber gun
- A five foot extension of the transom
- The addition of five blast hardened bulkheads

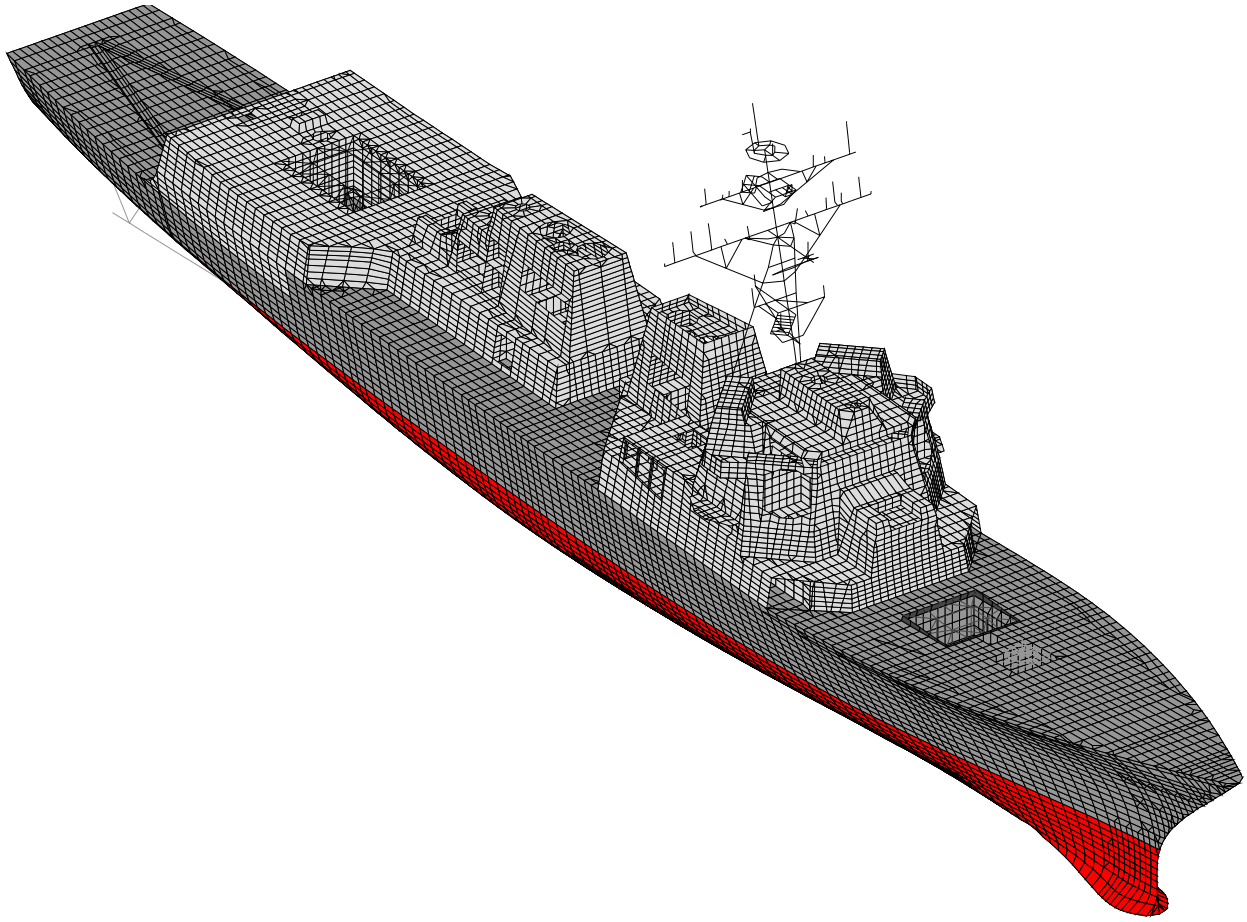

Figure 1. USS WINSTON S. CHURCHILL (DDG 81) FINITE ELEMENT MODEL [9].

Delivered in MSC/NASTRAN input deck form, this model represents the largest and most complex finite element ship model to date [14]. Though based on the DDG 53 model, this model was greatly improved. Structural beam elements were refined to reflect true areas, volumes, and densities and end-constraints were modified to better reflect actual structural boundary conditions. The mass distribution was improved significantly. Following completion of the model, nodal masses were added throughout the model to reflect such masses such as weapons loadout, liquid loading, equipment, and even personnel loading. Rather than the normal smearing of this mass arbitrarily onto the entire model, masses were distributed onto nodes in the model that corresponded to the associated mass on the actual ship. Since the three underwater shocks were accomplished on separate days, three separate models were delivered, each with a unique mass distribution applicable to the actual ship condition when the shot was conducted. Table 1 is a summary of this finite element model.

Complex equipment such as the gas turbine engines, shafts, generators, reduction gear, VLS launchers, and the gun mount were modeled as rigid body elements. Since the internal response of this equipment is not measured, modeling these individual components in detail is unnecessary. Each of these element groups was attached to the nodal points on the ship structure at their foundations with their spring-mass representation applied to the supporting nodes. To separate the propulsion shafts from the reduction gear, a beam element was added as a link between the two groupings. The shaft mass was then represented by each of the shaft bearing assemblies. Figure 2 shows the significant rigid body element groups. A total of 107 total rigid body element groups were in the final models used in the simulations. In addition to those shown, many of these groups were small groups of one, two, or three elements that make up antennas on the mast and the ship's Recovery, Assist, Securing, and Traversing (RAST) system located on the flight deck.

Table 1. DDG 81 Finite Element Model Specifications

Number of Nodes	40,514
Number of Degrees of Freedom	243,084
Number of Beam Elements	49,397
Number of Shell Elements	48,397
Number of Spring Elements	48,662
Number of Rigid Body Element Groups	107
Number of Lumped Masses	92,541

SHIP SYSTEM DAMPING REPRESENTATION

Ninety percent of damping in a structure occurs due to frictional energy dissipation in bolted or riveted mechanical joints. The vast majority of joints on naval combatant ship structure systems are welded while all stiffeners are welded directly to the hull plates, decks, and bulkheads. These welded joints provide minimal energy dissipation [15]. Regardless, many energy dissipation sources such as long cable trays, hangers, snubbers, and the surrounding fluid coupled with the hull are inherent to all ship systems. While ship system damping is measurable, it is difficult to quantify for modeling purposes. Extensive study was conducted at NPS in conjunction with the ship shock simulation of USS JOHN PAUL JONES (DDG 53) using 2000 msec of measured shock trial data [16]. The results of this study were applied to the Rayleigh damping coefficients used for the DDG 81 model.

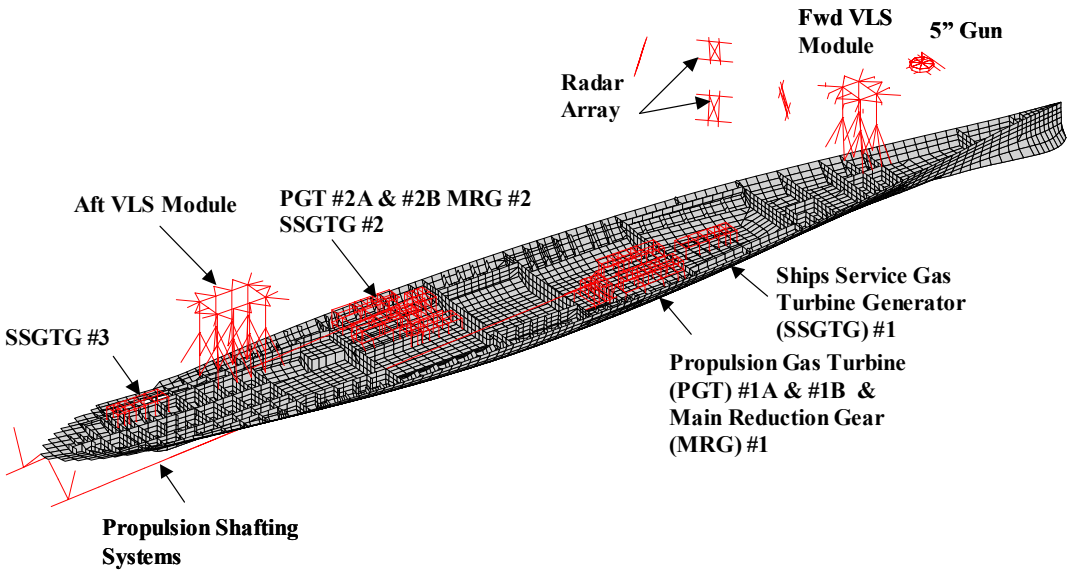

Figure 2. Equipment Modeled as Rigid Bodies in DDG 81 FEM [9]

Rayleigh damping is a general form of proportional damping representing the damping matrix, [C], in the structural equation of motion.

$$[M]\{\ddot{x}\}+[C]\{\dot{x}\}+[K]\{x\} = \{F\} \quad (1)$$

The [C] matrix is represented by

$$[C] = \alpha[M] + \beta[K] \tag{2}$$

where α and β are constants. This equation can be normalized using the mass normalization matrix $[\phi]$

$$[\phi]^T [C][\phi] = \left[2\zeta_\gamma \omega_\gamma\right]_{diag} = \alpha[I] + \beta\left[\omega_\gamma^2\right]_{diag} \tag{3}$$

Determining these damping coefficients for a simple system having only two modes with two modal frequencies of interest is academic. Determining them for complex systems such as a ship structure with more than two modes of interest presents a much greater challenge. In this case, Equation (3) becomes over determined, having more equations than unknowns. These coefficients can be determined using measured data and a least squares curve fitting technique with applying modal parameter extraction method[13].

For comparison with measured ship response the modal damping ratio is calculated. This is determined for each mode by

$$\zeta_i = \alpha\frac{1}{2\omega_i} + \beta\frac{\omega_i}{2} \tag{4}$$

DDG 53 was divided into 67 area groups for the comparison studies. Measured modal response was recorded over the entire frequency spectrum of interest, 0 to 250 Hz, for both athwartship and vertical response. A least squares curve fit was then applied and the corresponding α and β were recorded for each area. Figure 3 shows an example of this curve fitting for one area group. This particular plot includes the measured data outliers and "noise" that were subsequently discarded in performing the final curve fit.

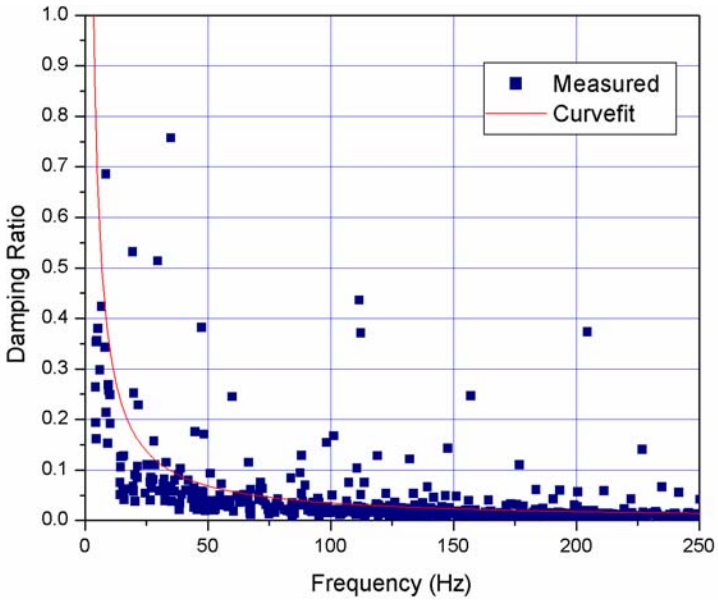

Figure 3. Vertical Modal Damping Ratio for Single Area Group of DDG 53 [16]

Each area group was given a weight based upon the number of modes used in determining the least squares curve fit for that area group. These values were summed and divided by the sum of the modes used to find both the weighted α_{mean} and the weighted β_{mean}. These values are shown in Tables 2 and 3. The recommended values for α and β for

DDG 53 were determined to be 19.2 and 2.09e-6 respectively. These values were chosen due to the fact that the vertical response is much larger in magnitude than the athwartship response. The resulting damping ratio curve for both response directions is shown in Figure 4 [13]. From a structural damping perspective, DDG 53 and DDG 81 are virtually identical. Due to this similarity these values were used for the DDG 81 model [13].

Table 2. Weighted Mean of α (DDG 53) [13]

Athwartship Direction	Vertical Direction
18.4	19.2

Table 3. Weighted Mean of β (DDG 53) [from Ref. 13]

Athwartship Direction	Vertical Direction
2.82E-6	2.09E-6

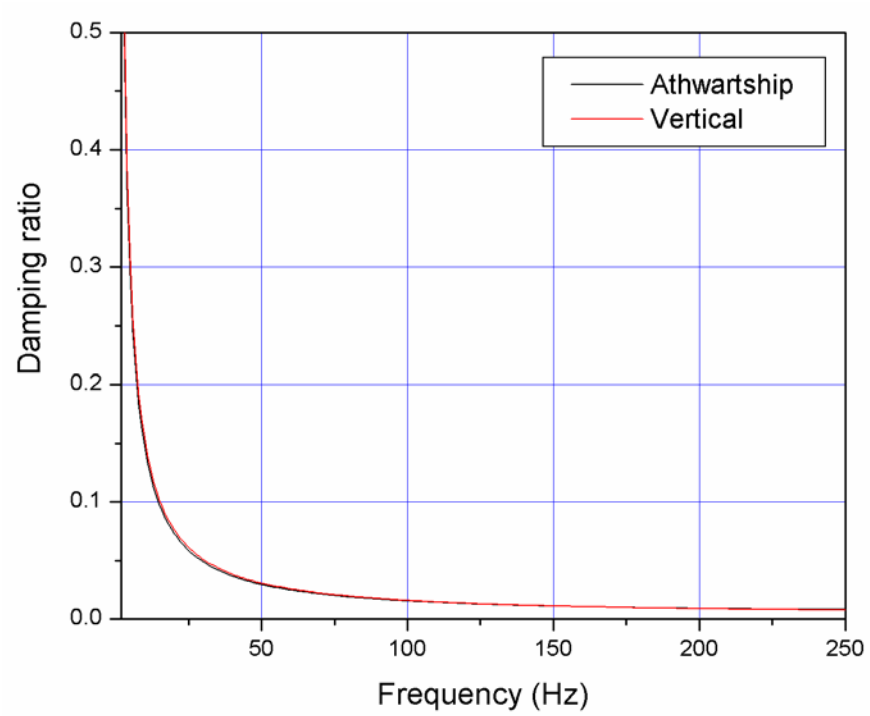

Figure 4. Frequency Dependent Damping Representation for DDG 53 Shock Data [16]

FEM SHIP MODEL GENERATION AND PRE-PROCESSING

Several analysis programs were used in the modeling and simulation of DDG 81. The model building, simulation, and data analysis procedure is shown in Figure 5. The USS WINSTON S. CHURCHILL structural finite element model was originally constructed by Gibbs & Cox, Inc. The model was in MSC/NASTRAN format and delivered in this form. MSC/NASTRAN/PATRAN was then initially used to identify elements and element properties and as a quality control check to verify all element and material properties were properly defined.

The actual simulations were performed using LS-DYNA coupled with USA. This required that the model be translated from NASTRAN format to LS-DYNA keyword format. This was a complicated, but critical step that was done through a local conversion code written in FORTRAN. For construction of the surrounding fluid model, the

structural model was imported directly into the TrueGrid mesh generator in NASTRAN format. More will be discussed on the construction of the fluid mesh using TrueGrid.

SIMULATION PROCESSING

LS-DYNA (Version 960) and USA were used to simulate the underwater shock and solve for the response of the structural model. LS-DYNA is a computational tool very popular in the automotive industry where it is commonly used to simulate such events as automobile crashes and airbag deployment. It is an explicit and implicit finite element program capable of analyzing the nonlinear dynamic response of three-dimensional inelastic structures [7].

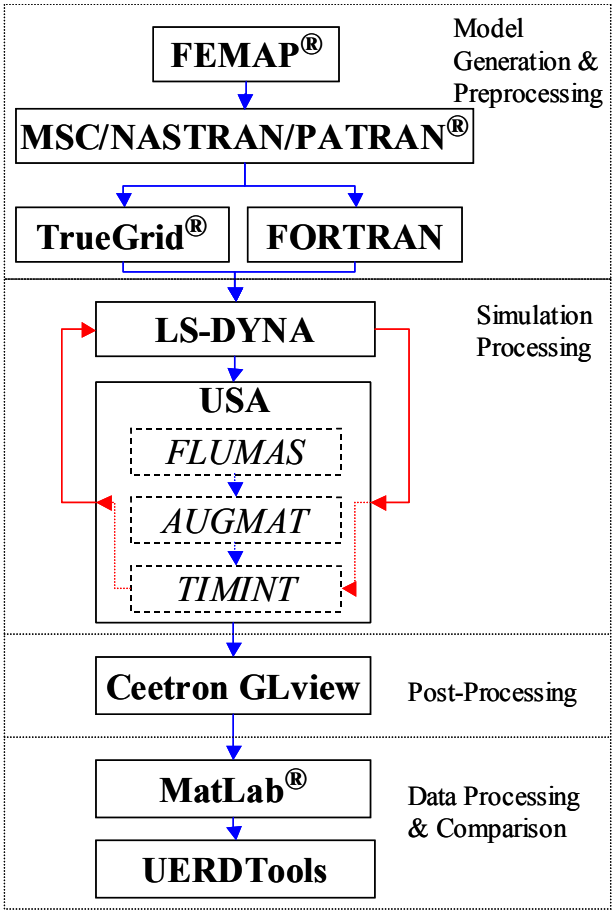

Figure 5. Model Generation and Simulation Flow Chart

Working in conjunction with LS-DYNA, USA was used to calculate the transient response of the ship's wetted surface structure to the incident shock wave. USA uses the Doubly Asymptotic Approximation (DAA) to solve the fluid structure interaction equations. This approximation method begins first with the structural equation of motion

$$[M]\{\ddot{x}\} + [C]\{\dot{x}\} + [K]\{x\} = \{f\} \tag{5}$$

where [M], [C], and [K] make up the symmetric linear structural mass, damping and stiffness matrices respectively and {f} is the external forcing vector. For a submerged structure excited by an acoustic wave this external forcing vector is

$$\{f\} = -[G][A_f]\{(p_I + p_S)\} + \{f_D\} \tag{6}$$

where $\{p_I\}$ and $\{p_S\}$ are the nodal incident and scattered pressure vectors respectively for the wetted surface structure, $\{f_D\}$ is the dry structure applied force vector, $[A_f]$ is the diagonal area matrix pertaining to the fluid elements, and [G] is the transformation matrix that relates the structural and fluid nodal surface forces. While the incident pressure vector is known, the scattered pressure vector is unknown [15].

The DAA is used to determine the fluid structure interaction. The DAA is so named as it approaches exactness in both the high-frequency (early time) and low frequency (late time) limits [19]. This approximation uses two equations, the structural equation of motion and a fluid particle equation,

$$[M_f]\{\dot{p}_s\} + \rho c[A_f]\{p_s\} = \rho c[M_f]\{\dot{u}_s\} \tag{7}$$

where $\{u_s\}$ is the scattered-wave fluid particle velocity vector normal to the structural wetted surface, $[M_f]$ is the symmetric fluid mass matrix for the fluid mesh on the wet surface, and c is the acoustic velocity. The DAA is able to represent the entire fluid surrounding a submerged structure through variables associated only with the wetted surface.

The fluid particle velocities are related to the structural response through the compatibility relation

$$[G]^T\{\dot{x}\} = \{u_I\} + \{u_S\} \tag{8}$$

This equation contains the constraint that the normal fluid particle velocity must match the normal structural velocity on the wet surface of the structure [16].

Equations (16) through (8) can now be combined to form two equations

$$[M_s]\{\ddot{x}\} + [C_s]\{\dot{x}\} + [K_s]\{x\} = -[G][A_f]\{(p_I + p_S)\} \tag{9}$$

$$[M_f]\{\dot{p}_S\} + \rho c[A_f]\{p_S\} = \rho c[M_f]([G]^T\{\ddot{x}\} - \{\dot{u}_I\}) \tag{10}$$

Equations (9) and (10) are solved using a staggered solution scheme in the Underwater Shock Analysis (USA) code in order to approximate the forces at the fluid structure interface [8]. These forces can then be input into a finite element solver to determine the structural response throughout the ship structure.

This method allows the problem to be solved without requiring a large fluid volume mesh. This works very well for incident shock wave predictions, but does not consider cavitation, making it ideal for structures not affected by cavitation such as a deeply submerged submarine.

Cavitation has a major impact on the response of a surface ship subjected to an underwater shock, particularly in the late time response. A fluid volume finite element model (FEM) must surround the ship an adequate distance in order to capture the effects of bulk and local cavitation. Previous studies have shown that the minimum depth of this fluid mesh should be at least one half the cavitation depth for a reasonable approximation [11,12]. This fluid volume model should be extruded from the wetted surface structure, matching the structural element faces and node points as perfectly as possible [20]. The DAA boundary is then placed on the outer surface of the fluid volume. This requires considerably more computational resources, but the improvement in the predicted response is substantial, making it a necessary requirement [21]. The USA code consists of three components; FLUMAS; AUGMAT; and TIMINT and the details are described in Ref. [8,18].

SIMULATION POST PROCESSING AND DATA EXTRACTION

After LS-DYNA and USA have completed processing the model, the data stored in the output files were extracted using GLview. GLview is a very capable 3D visualization and animation post-processor [23]. The simulations required tremendous quantities of data to be processed due to the extremely small calculation time step necessary. GLview is capable of handling these large quantities, producing a spectacular interactive animation of the virtual shock environment. In addition, it was used to download and display the structural response time history graphically. It served as an interface between the raw simulation data output from USA and the data comparison tools used to compare the simulation predictions with measured test results. These raw files were loaded into GLview and then structural response parameters such as nodal velocities and accelerations were exported as ASCII files for further analysis.

The nodal velocities and accelerations exported from GLview required filtering to remove undesirable frequencies. This was accomplished by importing the data files into a MATLAB code which processed the data through a low pass Butterworth filter. The data was then imported into UERD-Tools for comparison with measured shock trial data. UERD-Tools was developed by the Underwater Explosions Research Department (UERD), NSWC-Carderock Division in Bethesda, Maryland for the purpose of analyzing shock trial data. It has numerous features specific to ship shock analysis such as unit scaling of data, filtering, interpolation, time shift, and error criteria calculations.

FLUID MESH MODELING

Fluid mesh modeling is the one of focus of this paper. Several fluid models were constructed to model the three different shock environments. These models were all constructed using TrueGrid [5]. TrueGrid is a powerful mesh generator that allows meshes of all types to be created interactively. While its full capabilities cannot be overstated, one key feature that makes it ideal for modeling the underwater shock environment is its ability to extrude the fluid mesh through the structural mesh. This results in a fluid mesh that aligns perfectly with the structural mesh from the fluid-structure interface out to the Doubly Asymptotic Approximation (DAA) boundary. While several models were used in the simulations, all of these models were variations of just three models. The construction of the third model, an improvement over the first two models, is highlighted in this section.

The fluid mesh was constructed using essentially four subdivisions merged together; the inner liner, the inner mesh, the transitional mesh, and the outer mesh. By building the fluid mesh in this manner, several goals were accomplished:

- USA code stability criteria was met
- The fluid volume was meshed perfectly orthogonal to the structural mesh
- A quality mesh was maintained throughout the fluid volume from the fluid structure interface out to the boundary
- The fluid model was easily modified
- The proper waterline was achieved

INNER LINER

The inner liner of the fluid mesh serves as the fluid structure interface. It is the most critical part of the fluid mesh. The liner must mesh perfectly with the structural mesh, it must be as orthogonal to the hull as possible, and it must meet USA code stability criteria. Regardless of the quality of the remainder of the fluid mesh, a poorly constructed inner liner will result in a poor approximation. This segment of the fluid mesh consists of 37 subparts and accounts for approximately 50% of the fluid mesh model code written.

Mesh Stability Criteria: The nodal spacing of this inner liner is critical to the stability of the USA code. The code requires that the nodal spacing of this inner layer cannot exceed a defined thickness, D, given by the following equation:

$$\frac{2D\rho}{\rho_S t_S} \leq 5 \tag{11}$$

where ρ is the density of water and ρ_S and t_S are the density and thickness respectively of the wetted surface shell elements. The DDG 81 model wetted surface was constructed using a variety of quadrilateral and triangle shell elements. The shell thickness ranges from 0.375 inches to 1.25 inches. The material density of shell element is ρ_S=7.324E-4 (lbf-s^2/in^4) while the density used for the water is ρ=9.3601E-5 (lbf-s^2/in^4). Applying the values in Equation (11) results in the maximum allowable thickness of the inner liner being 7.33 inches. To ensure that this was not exceeded, a thickness of seven inches was used for the entire inner liner.

Orthogonality: The majority of the inner liner was made orthogonal to the hull by using TrueGrid's "BLUDE" command along with the "NORMAL" command. The BLUDE command extrudes the fluid mesh through the structural mesh resulting in a fluid mesh which is merged perfectly with the structural mesh. While the BLUDE command does generally achieve normality, the NORMAL command was used to ensure that the fluid mesh was normal to the hull over its entirety and only seven inches in thickness. The abrupt structural transitions such as the keel, bow, sonar dome, and stern areas did not allow for a single continuous fluid liner to be extruded from the hull. In these areas the liner was first extruded on all faces around the transition area. The gaps that were left between these meshes were filled in using wedge shaped elements. This ensured that orthogonality was maintained at these transitions while filling in the gap to allow for further construction of the fluid mesh.

Waterline: The proper waterline is essential for two reasons, to ensure proper global orientation of the fluid model and to accurately model the fluid structural interface. The DDG 81 structural model was constructed without mesh lines at the test waterline. To ensure that the fluid mesh was merged properly with and orthogonal to the structural mesh at the waterline, wedge shaped elements were constructed to transition from the structural mesh line to the actual waterline. Fluid-structure orthogonality was compromised in the aft section of the ship due to the extreme transition from the structural mesh line to the test waterline. To minimize this compromise, an additional layer was constructed to encapsulate the inner liner and continue the transition to the test waterline in this area. This second layer was eight inches in thickness, bringing the total thickness of the inner liner to fifteen inches nominally. Figure 6 shows the completed fluid mesh two layer inner liner.

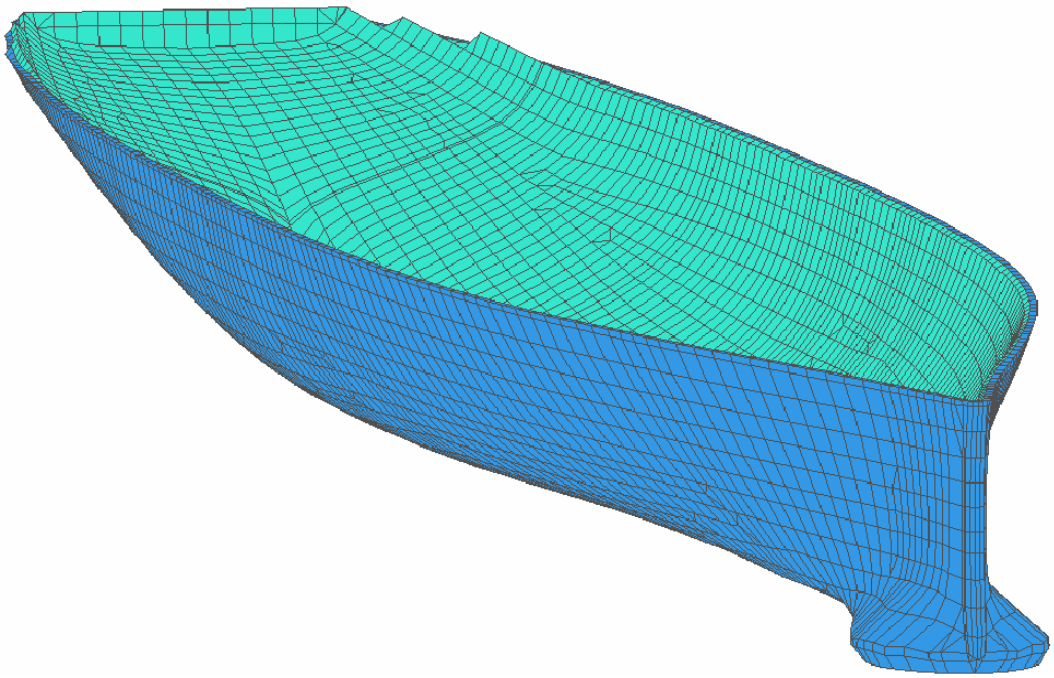

Figure 6. Fluid Model Two Layer Inner Liner

INNER MESH

Many of the contours of the ship, particularly the sonar dome region and areas around the keel, form concave surfaces and have sharp transition areas. The purpose of this inner mesh is to provide a transition from these complex contours of the structural model to a surface convex in nature. The quality of the entire fluid mesh depends greatly upon the quality of this region. Complex control of the fluid mesh through the use of proper vertices placement, curve attachments, and surface projections is key to constructing this region of the mesh. Proper use of mesh interpolation methods is essential in this region to obtain a quality mesh. TrueGrid uses several interpolation techniques to ensure a quality, uniform mesh.

Thomas-Middlecoff Relaxation: Using linear iteration as described in Ref. [21], Thomas-Middlecoff relaxation (TME) improves the mesh by solving a Poisson equation. This relaxation method excels in propagating the edge's nodal distribution into the interior of the mesh. In doing this, it attempts to maintain orthogonality throughout the mesh [6].

Equipotential Relaxation: This method of mesh interpolation treats the mesh lines as solutions to the Laplace equation with the boundary conditions formed by the boundary nodes. This allows the interior volume of a mesh to be relaxed while maintaining the boundary nodal distributions. The primary purpose of using this interpolation method is to maintain a defined boundary while producing a uniform interior mesh [6]. The inner mesh was constructed to allow for variation of mesh density, allowing the number of elements between the inner and outer boundaries to be changed using parameters. In its entirety, five separate subparts were constructed separately and merged together to form this region of the fluid model. The finished inner mesh extended outward a nominal distance of five feet from the inner liner. It is shown in Figure 7.

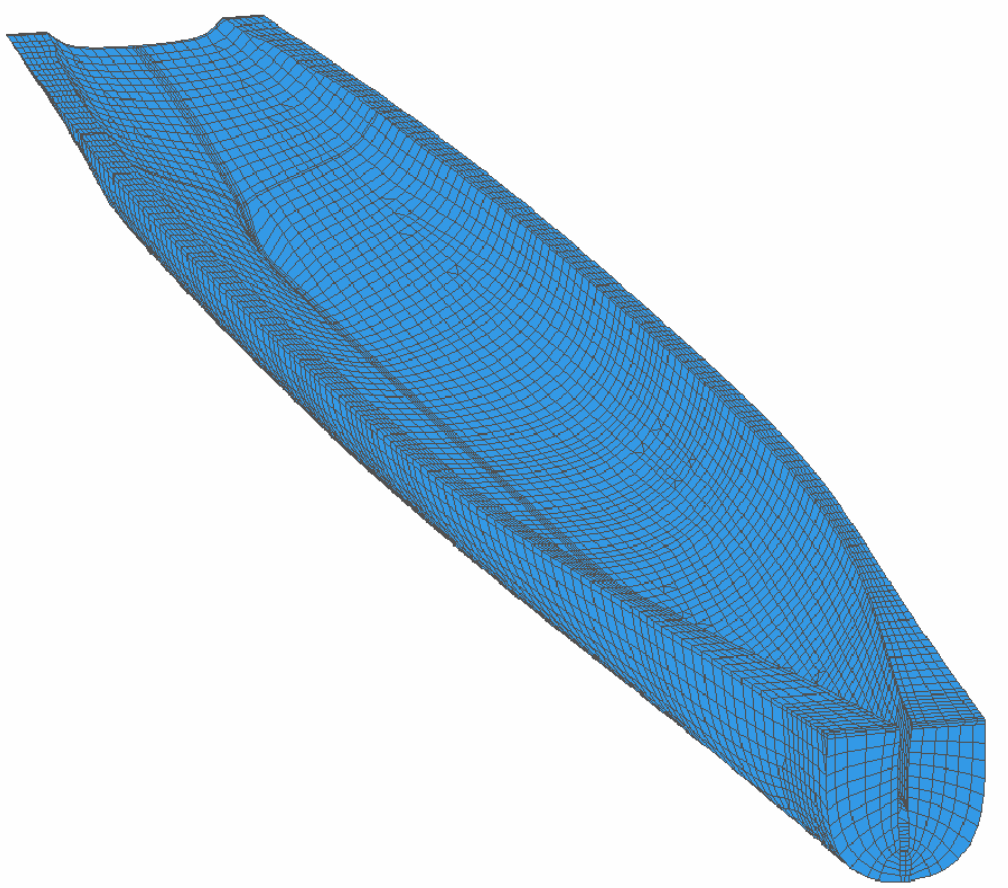

Figure 7. Fluid Model Inner Mesh

TRANSITIONAL MESH

The transitional mesh encapsulates the inner mesh and extends out to approximately ten feet from the hull. Conical shaped mesh regions were used to extend the bow and stern areas outward to merge perfectly with the contoured outer boundary of this mesh.

The fluid model has the ability to model the underwater shock environment for DDG 81 under varying loading conditions by allowing the waterline to be adjusted. The ability of the model to adjust to these different conditions occurs in this region of the mesh. This is accomplished by allowing the inner mesh to "float" along with the ship model inside this transitional mesh. The transitional mesh then transitions from the fixed 258 inch waterline of the inner mesh to the actual test waterline. The simulations investigated in this paper all had a test waterline of 258 inches fore and aft which the inner liner and mesh was initially designed for. This feature was not necessary in these simulations, but was added to allow for future underwater shock simulation modeling of DDG 81.

In addition to allowing for variation in waterline, this region also allows for variation in mesh density. It consists of three parts constructed separately and merged together and with the previously constructed fluid model. The finished transitional mesh is shown in Figure 8.

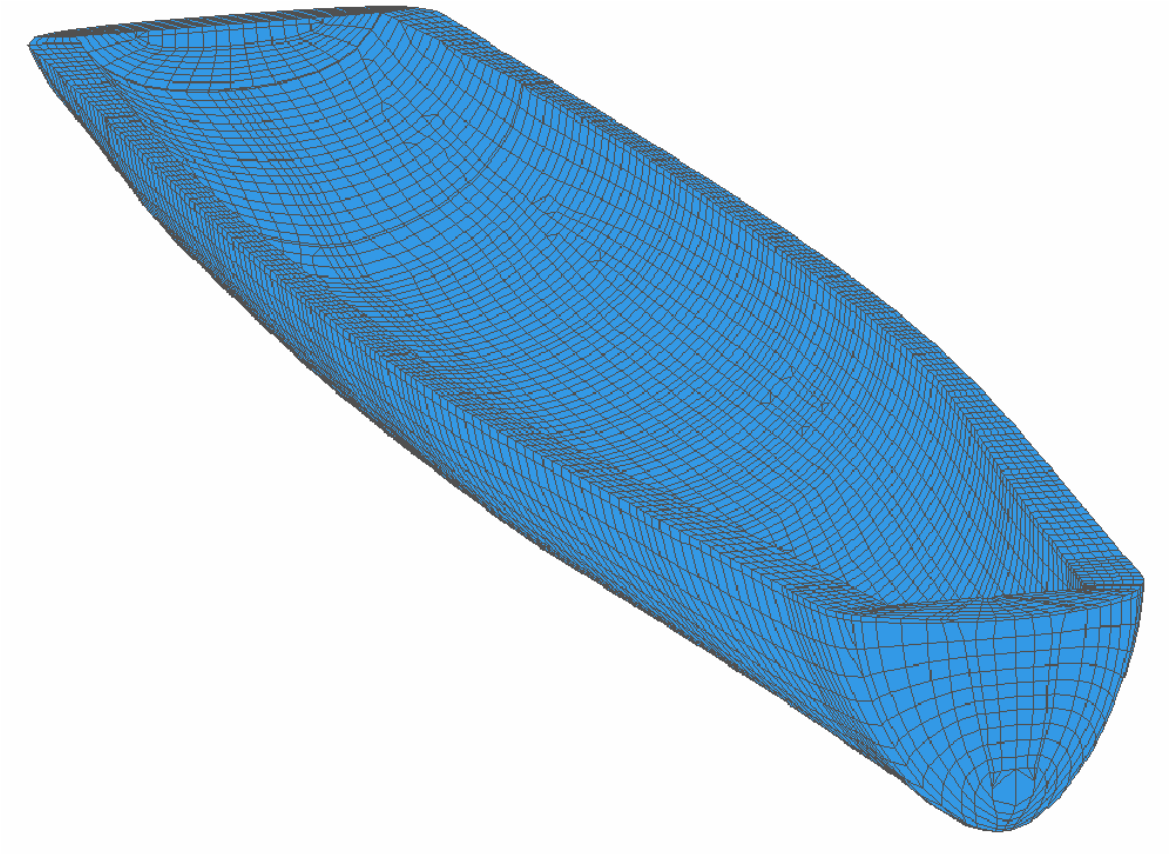

Figure 8. Fluid Model Transitional Mesh

OUTER MESH

The outer mesh extends the fluid volume out to the DAA boundary. The DAA boundary is formed on the outer surface of this mesh by selecting the outer faces of this mesh. Constructed to allow for the simulation of virtually any underwater shock environment, the depth, fluid mesh density, waterline, and contour of this outer mesh can be modified with just a few simple parameter inputs. Though comprising the majority of the fluid model, this region

was constructed using only one part. The completed outer mesh is shown in Figure 9. The complete coupled fluid structure model is shown in Figure 10.

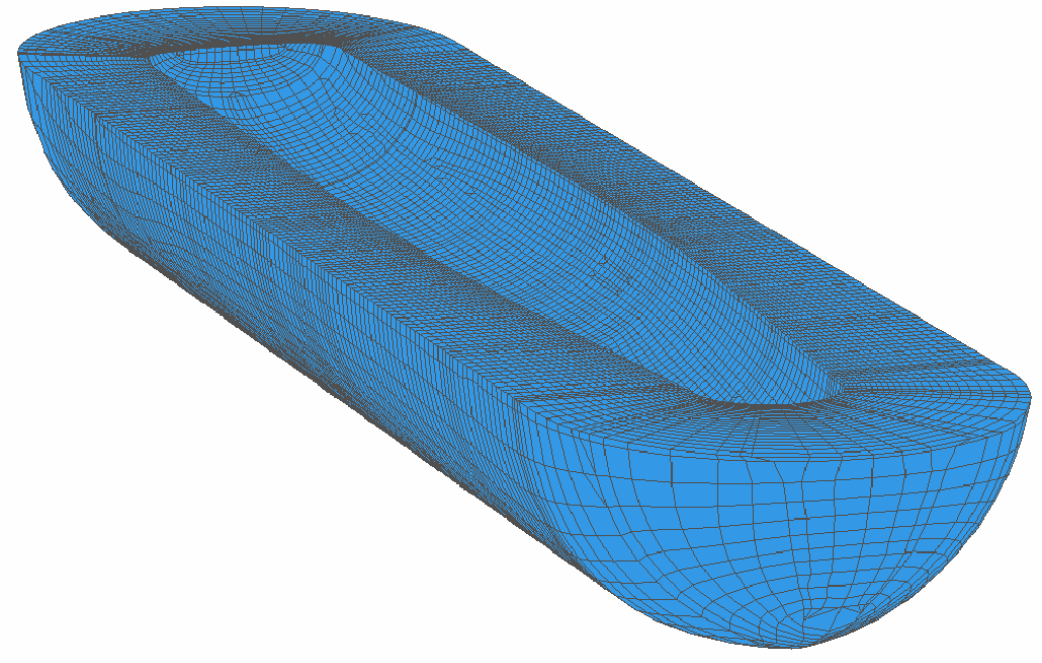

Figure 9. Fluid Model Outer Mesh

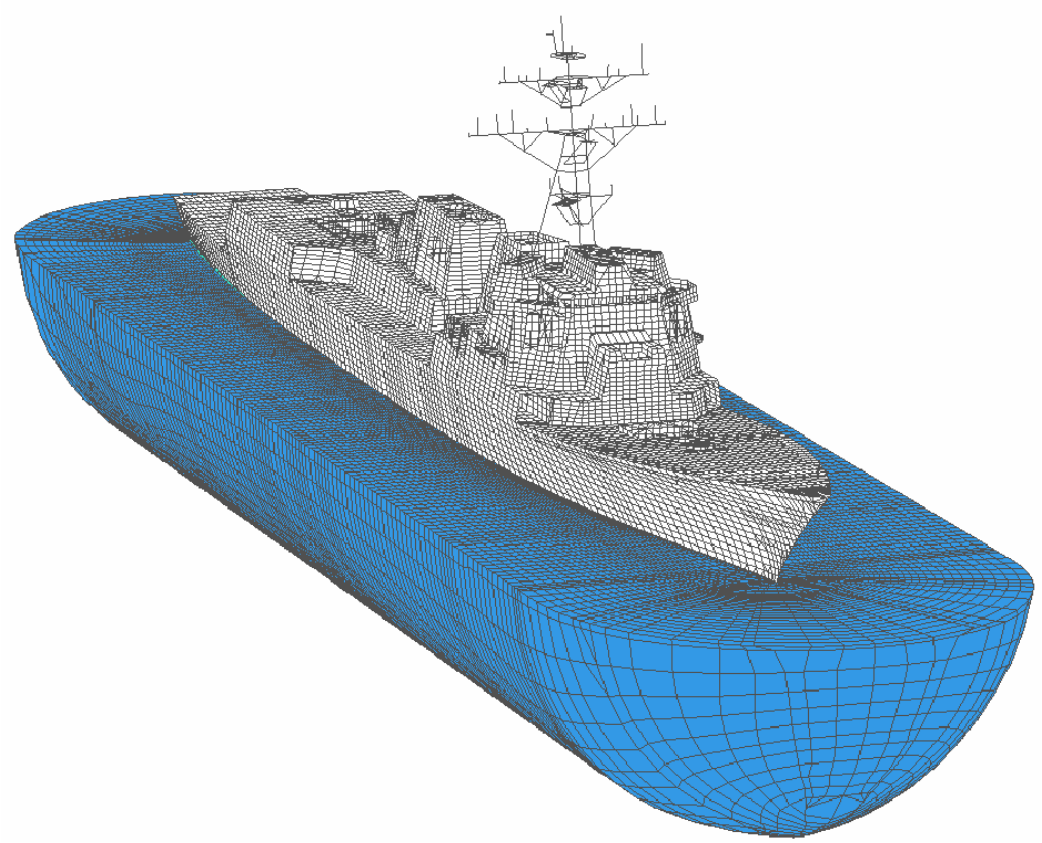

Figure 10. Complete Coupled Fluid-Ship Model

DATA COLLECTION AND ANALYSIS

Many variables exist in the underwater shock environment, one of those being the method in which the measured data is collected and analyzed. Prior to making any comparisons with simulation predictions, the data must be properly analyzed. The existence of low frequency "drift" and high frequency "noise" in shock trial data present a formidable challenge to overcome.

VELOCITY RESPONSE "DRIFT"

the velocity meter and accelerometer were originally intended for measuring short duration transient motion signals over a limited frequency bandwidth. The accelerometer is ideal for frequency response measurement at frequencies far below its own resonant frequency while the velocity meter is more suitable for measuring the response to frequencies far above its own resonant frequency [25]. For purposes of underwater shock simulation measurement it is desirable to extend the measurement time out to capture more of the response. This results in requiring the sensors to measure a considerably larger range of frequencies than they were intended for. Velocity and displacement time histories acquired by integrating acceleration time histories have a tendency to drift due to errors in the zero reference portion of the time history. This problem exists as well in velocity meter time history as velocity meters require seismic correction, which involves integration as well. As a result, the measured data displays a substantial amount of drift as shown in Figure 11. The primary and dominant direction of ship motion is vertical regardless of charge location and vertical velocity response is considered here.

A significant amount of study was conducted to determine how to eliminate this drift. UERD-Tools has a built-in function called "Drift Compensation" which uses an algorithm to eliminate this drift. Figure 12 shows the same velocity data after this drift compensation has been used. The advantages of using this technique are that the magnitude of the response is maintained and there is no shift in phase. The disadvantages are that it does not always eliminate the drift as shown in Figure 12. Further curve fitting where the analyzer uses his/her own judgment to determine where the data begins to drift is often required. This requires the user to determine a best-fit polynomial to the spurious trend. This polynomial curve is subsequently subtracted from the data. This technique has proven to be effective in "cleaning" the data, but it invites a fair amount of subjective interpretation and potential for biased modification of the data. Ideally, a method involving less "hands-on" manipulation of the data would be preferable.

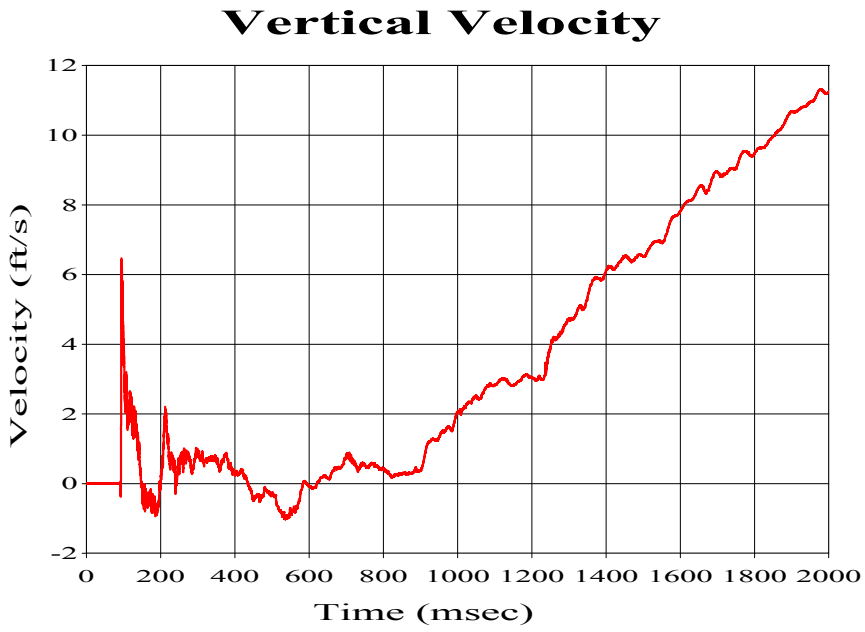

Figure 11. Raw Velocity Data Showing Drift

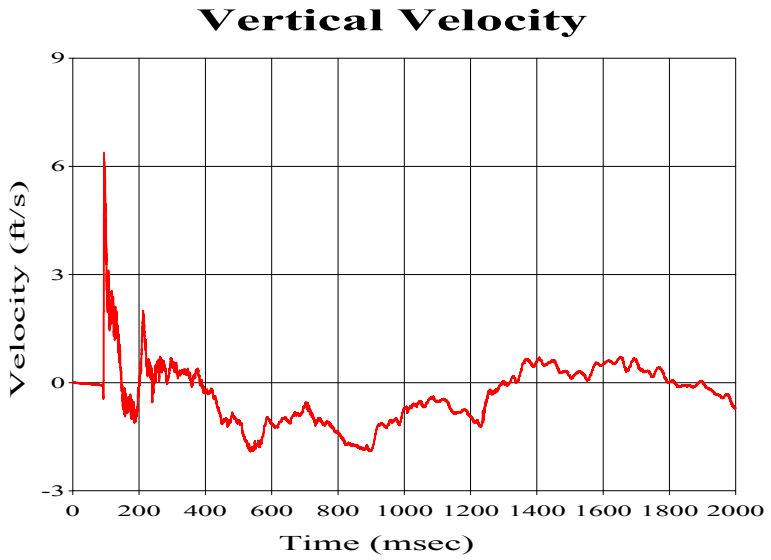

Figure 12. Velocity Data after Drift Compensation Has Been Applied

An alternate method of dealing with this drift is to process the data through a high-pass filter. While velocity meters record the global response, it is most desirable to determine only the local response at a particular location. To determine the local response it is therefore desirable to eliminate any rigid body modes from the sensor response. This can be measured by analyzing the late time displacement response of the structure where rigid body modes reveal themselves in the form of a non-zero steady state displacement. Doing this rigid body motion study for a number of sensors, it was initially determined that the measured data should be filtered using a Bessel two-pole high-pass filter set at a cut-off frequency of 3Hz. The same was done with the simulation data where a cut-off frequency of 1.8Hz was necessary. A two-pole Bessel filter was chosen as it is the only built-in high-pass filter in UERD-Tools. Figure 13 shows a comparison of filtered versus drift compensated velocity data. Filtering results in a velocity plot wit no significant drift apparent, while the drift compensated data still shows strong evidence of low frequency drift.

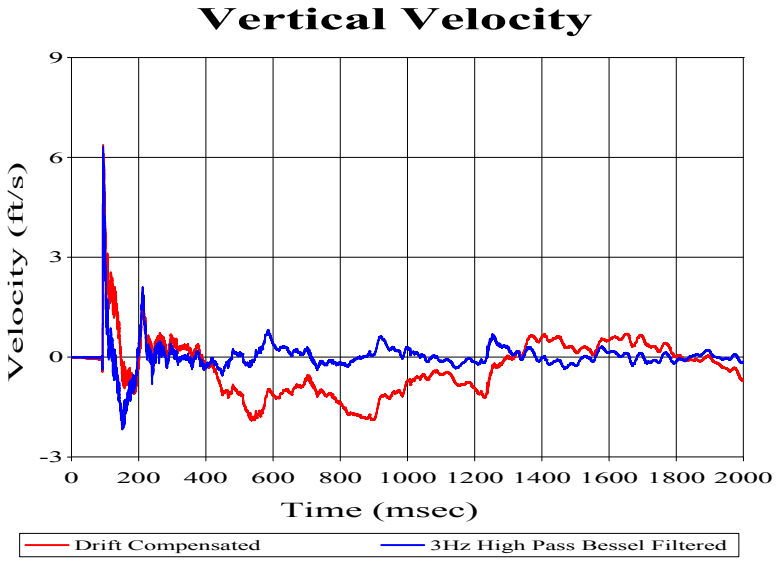

Figure 13. Comparison of High Pass Filtering vs. Drift Compensation

The disadvantage of using this high-pass filter is that desirable frequencies above 3Hz are filtered out due to the characteristic of the two-pole Bessel filter. Lowering the cut-off frequency to 0.5Hz results in less unwanted filtering, but as with drift compensation, evidence of rigid body motion still exist afterwards. A third-order high-pass Butterworth filter has a preferable high-pass characteristic. As shown in Figure 14, a third-order Butterworth filter reduces the amount of desirable frequency response that is filtered, but still has a small effect on the low frequency response. Figure 15 shows the result after applying a 0.5Hz cut-off to the data using a Butterworth filter. A small amount of low frequency drift is still apparent.

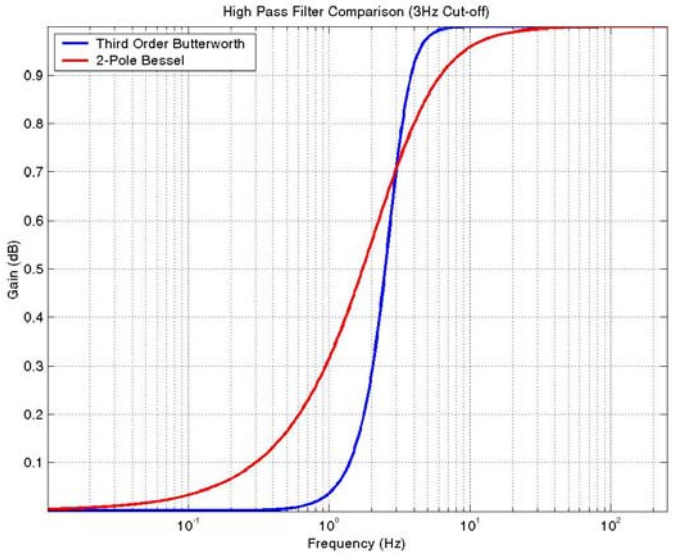

Figure 14. Butterworth vs. Bessel High Pass Filter with 3Hz Cut-off Frequency

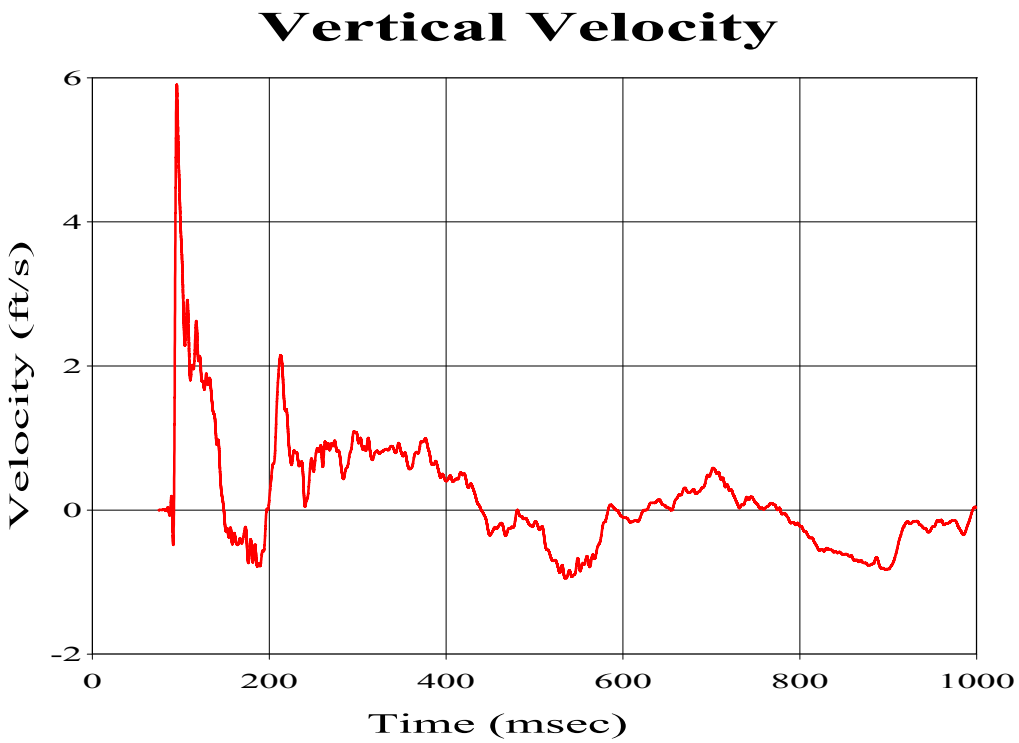

Figure 15. Velocity Response with 0.5Hz High-Pass Butterworth Filter (Third-Order)

HIGH FREQUENCY "NOISE"

In addition to drift, raw shock trial data has a fair amount of high frequency "noise" which clutters the data. The high frequency response is not of concern in UNDEX. These high frequencies are filtered out using a 250Hz cut-off low-pass filter. Figure 16 shows an example of the effects this filtering has on the data.

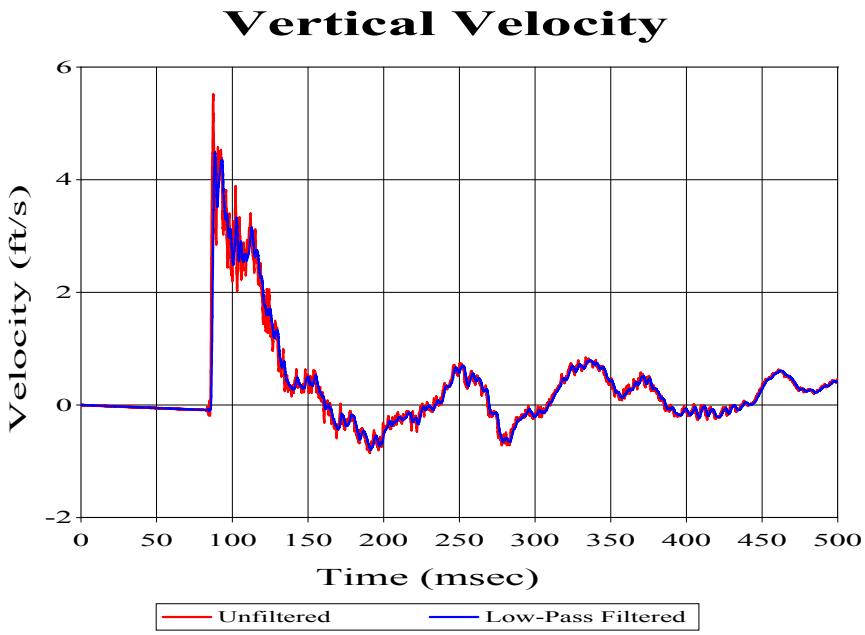

Figure 16. Effect of Low-Pass Filtering Data

SIMULATION RESULTS AND ANALYSIS

Three underwater explosions, shots, were conducted during the DDG 81 shock trials. The most severe of these shots was the third shot, "Shot 3", while the least severe shot was the first shot, "Shot 1". All three of these shots have been simulated using the FEM ship model coupled with several surrounding fluid models. The one of focus in this paper is to investigate the effects of fluid mesh density, the number of elements between the outer DAA boundary and the fluid-structure interface, and the ability to accurately simulate different shot geometries. In addition to this, the effects of varying mesh quality and fluid volume depth are investigated.

Sensor/Node Location: Over 600 sensors were mounted onboard DDG 81 to measure the response during each shot conducted. These sensors consisted of accelerometers, velocity meters and strain gauges. For comparison purposes, corresponding nodes were built into the structural model representing these sensors. During an underwater shock event, the primary structural response is in the vertical direction. For this reason, the vertical velocities were used primarily for the comparisons discussed in this paper. For vertical velocity comparisons, 32 sensors were compared for Shot 3, 30 for Shot 2, and 28 for Shot 1. While the majority of these sensors were vertical velocity meters, several accelerometers were used as well. The accelerometer data was subsequently integrated for comparison with predicted velocity response.

Error Measurement: Quantifying how well a calculated transient response compares to a measured response is very subjective. One way to eliminate any bias from the comparison is by using an impartial error measure such as Russell's error factor. Russell's error factor evaluates the magnitude and phase errors separately, combining the two to form a single comprehensive error factor [26].

The relative magnitude error is found by first forming two variables,

$$A = \sum_{i=1}^{N} f_1(i)^2 \tag{12}$$

and

$$B = \sum_{i=1}^{N} f_2(i)^2 \tag{13}$$

where $f_1(i)$ and $f_2(i)$ are the measured and predicted response magnitudes respectively at a given time step, i. The two variables can then be used to find the relative magnitude error,

$$m = \frac{(A-B)}{\sqrt{AB}} \tag{14}$$

The phase error contributes significantly to the error between two transient responses. If $\hat{\phi}$ is allowed to be the normalized unit vector of a transient response, the phase correlation between the measured and predicted responses can be defined by,

$$p = \hat{\phi}_1 \bullet \hat{\phi}_2 \tag{15}$$

Since the unit vectors are normalized, the values of p can range from –1.0 to 1.0 where –1.0 indicates that the two responses are completely out of phase, while 1.0 indicates that they are completely in phase.

A measure of the phasing between two transient response vectors in terms of correlation can be found by defining a new term,

$$C = \sum_{i=1}^{N} f_1(i) f_2(i) \tag{16}$$

The phase correlation between the two responses can then be computed by

$$p = \frac{C}{\sqrt{AB}} \tag{17}$$

It is important to note that p represents the phasing correlation between the two responses, it is not a measure of phase error. To calculate phase error, the following equation is used:

$$RP = \frac{\cos^{-1}(p)}{\pi} \tag{18}$$

The phase error factor has an error range of 0.0 to 1.0 where 0.0 indicates both responses are completely in phase while 1.0 indicates they are completely out of phase.

Although the phase error factor has a maximum value of 1.0, the relative magnitude error factor is unbounded. Since the two are combined to form the comprehensive error, it is easy to see that the magnitude error could easily dominate the comprehensive error, presenting an undesirable bias. To apply a similar bound to the magnitude error factor the following magnitude error factor is defined:

$$RM = \text{sign}(m)\log_{10}(1+|m|) \tag{19}$$

This maintains the sign unbiased nature of m while effectively artificially bounding the magnitude error factor since a RM value of 1.0 represents an order of magnitude error between the two responses. The comprehensive error factor can now be determined using the following equation:

$$RC = \sqrt{\frac{\pi}{4}\left(RM^2 + RP^2\right)} \tag{20}$$

where the $\frac{\pi}{4}$ term is a scale factor found by calculating the area of a square with a width of length RM and height of length RP. A circle with a corresponding area has a radius equal to $\frac{\pi}{4}$ times the diagonal of the square [23]. The comprehensive error factor is not bounded, but errors in excess of 1.0 indicate substantial error between data sets and virtually no correlation.

Russell's error factor allows an unbiased error value to be assigned to the correlation between the measured and predicted transient responses. The determination as to what justifies an acceptable or unacceptable prediction is more subjective however. It has been suggested that the values outlined in Table 4 should be used for acceptance criteria of a 500 ms processed velocity data comparison [24]. Processed data in this sense means both measured and predicted response data low pass filtered with a cut-off frequency of 250 Hz and measured data drift compensated to remove gauge drift. This acceptance criterion is not valid for shorter duration comparisons or data which has been processed using other techniques [25].

Table 4. Russell's Comprehensive Error Factor Acceptance Criteria

$RC \leq 0.15$	EXCELLENT
$0.15 < RC \leq 0.28$	ACCEPTABLE
RC>0.28	POOR

It should be noted that this acceptance criteria is only an agreed upon means of determining an acceptable or unacceptable prediction. While these error factors present a useful tool for statistical comparison between models, there are no magical lines of distinction drawn at the levels of acceptance. This is to say that a comparison resulting in a comprehensive error factor of 0.148 placing it in the "Excellent" category is not significantly better than an "Acceptable" comparison resulting in a comprehensive error factor of 0.152. Similarly, though unacceptable, a comparison resulting in a 0.285 error factor is not significantly worse than one whose comprehensive error factor is 0.275, an "Acceptable" value. With this in mind, comparisons should be summarized using the actual error factor values, not the subjective ratings applied to those numbers.

SEVERE SHOCK (SHOT 3)

The most severe shock conducted on DDG 81 was Shot 3. A diagram showing the relative aspect of this shot to the ship is shown in Figure 17.

SURROUNDING FLUID DEPTH STUDY: FIRST GENERATION FLUID MODELS

The initial focus of the investigations discussed in this paper was to determine the effects of surrounding fluid depth on the accuracy of the simulation predictions [29]. Four models were developed, a 15 inch thick two layer inner

liner fluid mesh, a half-cavitation depth fluid mesh, a cavitation depth fluid mesh, and a fluid mesh having a depth twice the cavitation depth. This comparison used Shot 3 exclusively as it was the most severe shock, producing the largest response magnitudes.

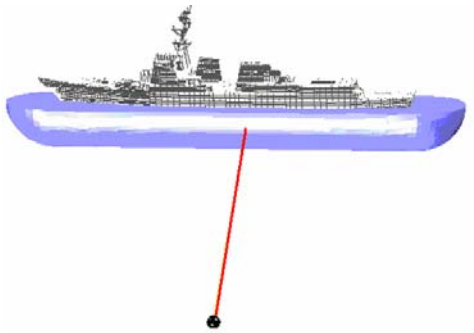

Figure 17. Shot 3 Geometry. Most Severe Shot, Charge Off Port Midships

Two-Layer Inner Liner Fluid Mesh: The two-layer inner liner fluid mesh model is same as shown in Figure 6. It consists of a seven-inch thick inner layer that is encased in an eight-inch thick outer layer. This fluid mesh constitutes the smallest fluid model used in the simulations. The inner liner fluid model does not accurately predict the structural response to the shock wave. Over half of the 21 sensors compared had a comprehensive error factor over 0.30 and none had comprehensive error factors below 0.20. The errors were significant in both phase and magnitude, though the phase error did dominate the majority of the comparisons.

One-Half Cavitation Depth Fluid Mesh: The second fluid model compared extended the depth of the fluid out to approximately one-half of the cavitation depth. This model is shown in Figure 18. The comparisons of this fluid model simulation show significant improvement over the inner liner fluid model simulation comparison. Significant errors still exist in the comparison with 9 of the 21 comparisons having a comprehensive error factor over 0.30. A third of the comparisons however had a comprehensive error factor less than 0.20, over half of these below 0.15. Though better than the inner liner fluid model simulation predictions for the most part, using this fluid model in the simulation does not result in predictions that are consistently accurate.

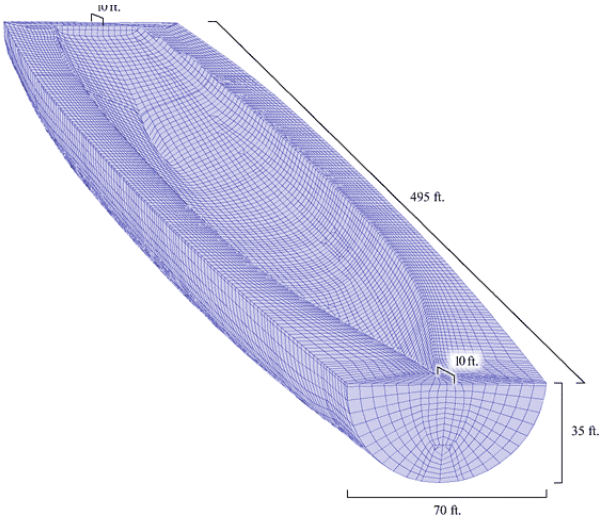

Figure 18. One-Half Cavitation Depth Fluid Mesh [26]

Cavitation Depth Fluid Mesh: The third fluid model compared had a depth approximately equal to the cavitation depth of the actual shot. Although the outer boundary of the fluid model is perfectly cylindrical, the cavitation depth changes along the length of the ship. Due to this, a perfectly cylindrical fluid model can only approximate the cavitation depth and, in this case, was modeled having a sufficient depth to include the cavitation region throughout the length of the ship. This fluid model is shown in Figure 19.

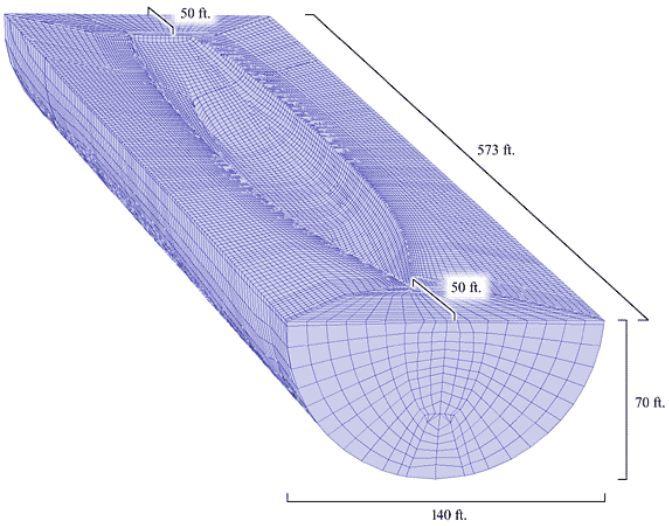

Figure 19. Cavitation Depth Fluid Mesh [29]

These comparisons show substantial improvement over the previous two simulation prediction comparisons. Only one comparison has a comprehensive error factor greater than 0.30 and 19 of the 21 comparisons have comprehensive error factors less than 0.20, 14 below 0.15, and 4 below 0.10. The majority of the error is due to the phase error as the majority of the magnitude errors are very small. From these comparisons, it is clear that the fluid model should be extended out to the cavitation depth to accurately predict the initial 120 msec response of the structure.

2X-Cavitation Depth Fluid Mesh: The exceptional correlation using the cavitation depth fluid mesh and the poor correlation using the smaller fluid mesh models indicates that there is at least a minimum depth constraint for the fluid model. To determine the sensitivity of fluid volume effect, a fluid model having a depth equal to approximately twice the cavitation depth was used to conduct a simulation. The comparison shows that the results did not improve. It may be caused by the fact that the size of fluid volume element is larger in radial direction and loosing the refined definition of incident pressure wave.

FLUID MESH DEPTH SENSITIVITY: SECOND GENERATION FLUID MODEL

The cavitation depth models used in the previous simulations were constructed having a depth of 840 inches as a rough approximation to the actual cavitation depth. This was to account for the greatest cavitation depth, that depth at a point on the ship's keel furthest from the charge. The cavitation depth at the point on the keel closest to the charge was found to be only 738 inches for this shot. Simulations conducted using a similar model, but with a reduced depth, resulted in a decrease of over 0.01 in the average Russell's comprehensive error factor. This suggests that the simulation is particularly sensitive to small changes in the depth of the fluid modeled. This model was subsequently modified, retaining the initial inner liner and majority of the inner mesh while replacing the flat end caps with spherical end caps. This modification eliminated the need for multiple parts in the outer fluid mesh, facilitating more efficient modification of the outer fluid mesh, and improved the fluid model's applicability to a wider variety of underwater explosion geometries. No appreciable change in the average error factors occurred from this modification. This second generation model is shown in Figure 20.

The best correlation achieved using the model shown in Figure 20. This was done using a densely packed fluid mesh where the average hull normal spacing between elements was less than 12 inches. Compared with the original 1st generation model, the improvement in the average comprehensive error was over 0.02, a significant reduction.

Fluid Mesh Quality: After several simulations were conducted and compared using the second generation model, a third generation model was developed in an attempt to improve the simulation predictions. Retaining only the inner liner from the first two models, this model focused on eliminating the "trouble spots" on the 1st and 2nd generation

models where the fluid mesh was extremely non-uniform, particularly the areas surrounding the sonar dome and skeg as shown in Figures 21 and 22. This fluid mesh also utilized the interpolation methods discussed in earlier section more heavily than the first two models. The end result is that this model had an improved mesh quality over the previous two models.

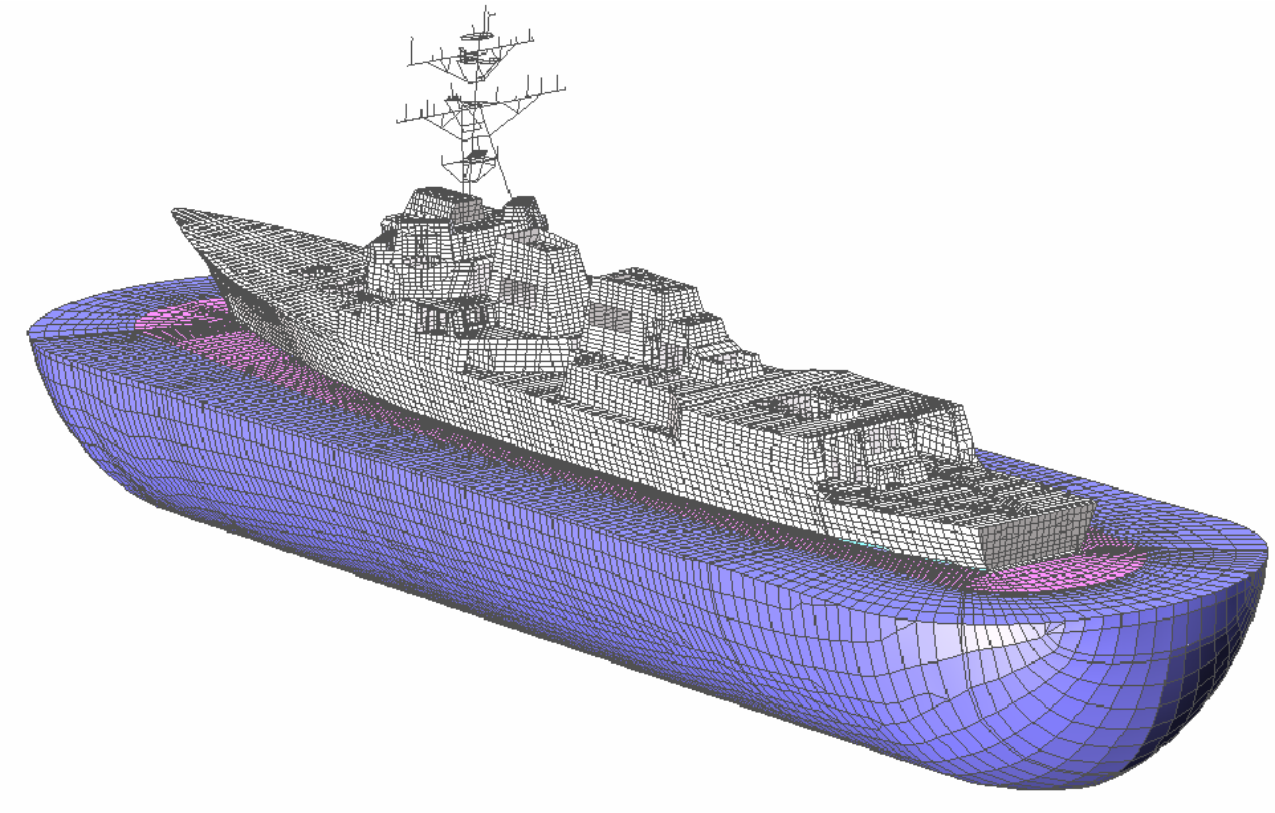

Figure 20. Second Generation Coupled Ship and Fluid Model

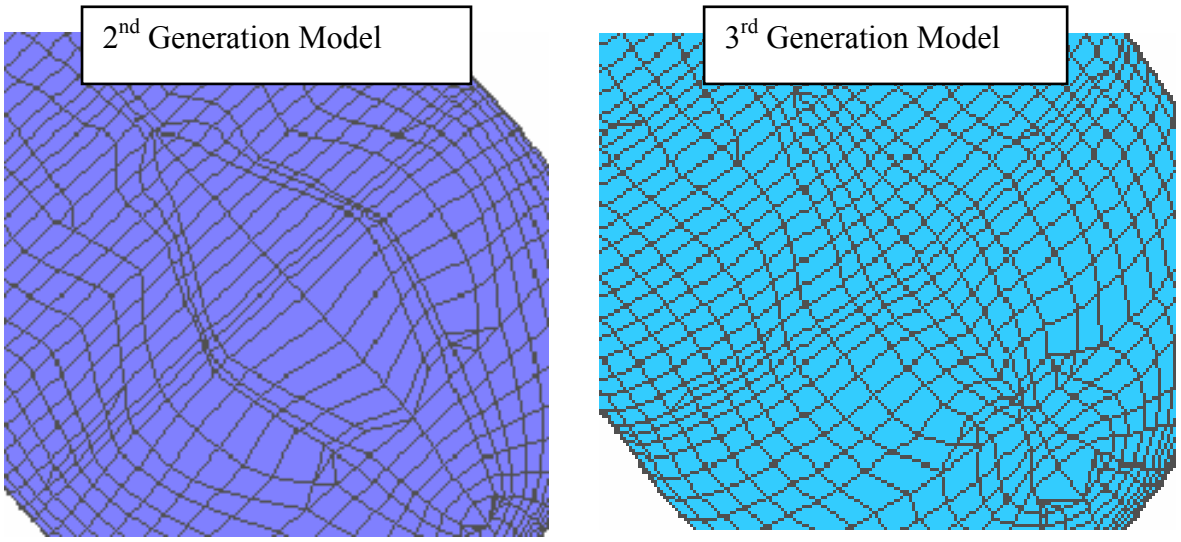

Figure 21. Sonar Dome Region Showing Improvement in Mesh Uniformity of 3rd Generation Fluid Model.

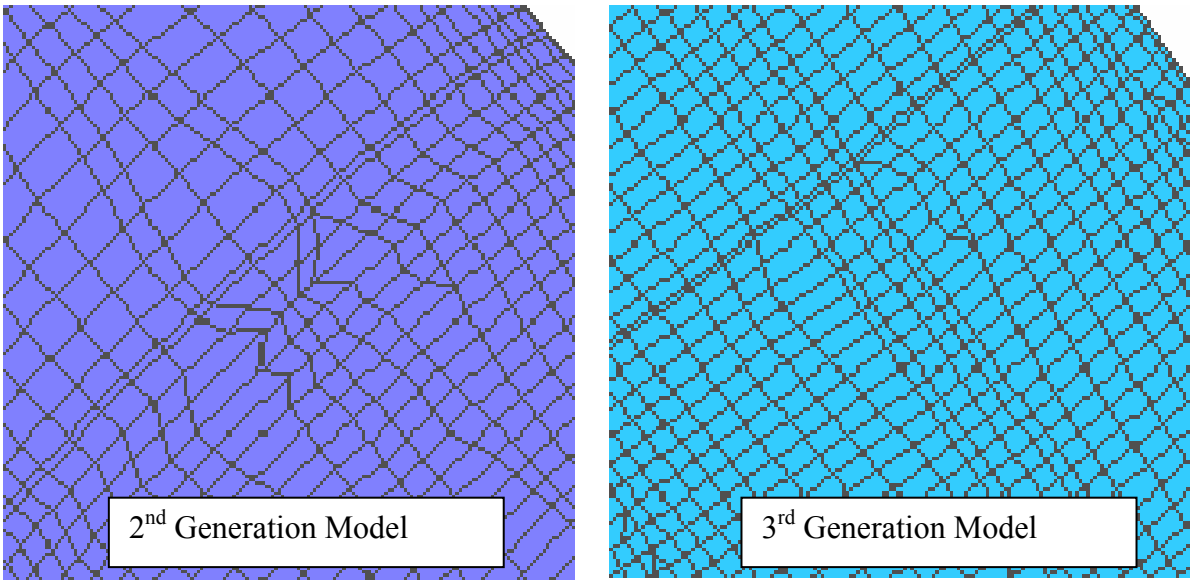

Figure 22. Keel Region Showing Improvement in Mesh Uniformity of 3rd Generation Fluid Model

A graphical comparison of the comprehensive error trend lines is shown with respect to location along the ship in Figure 23.

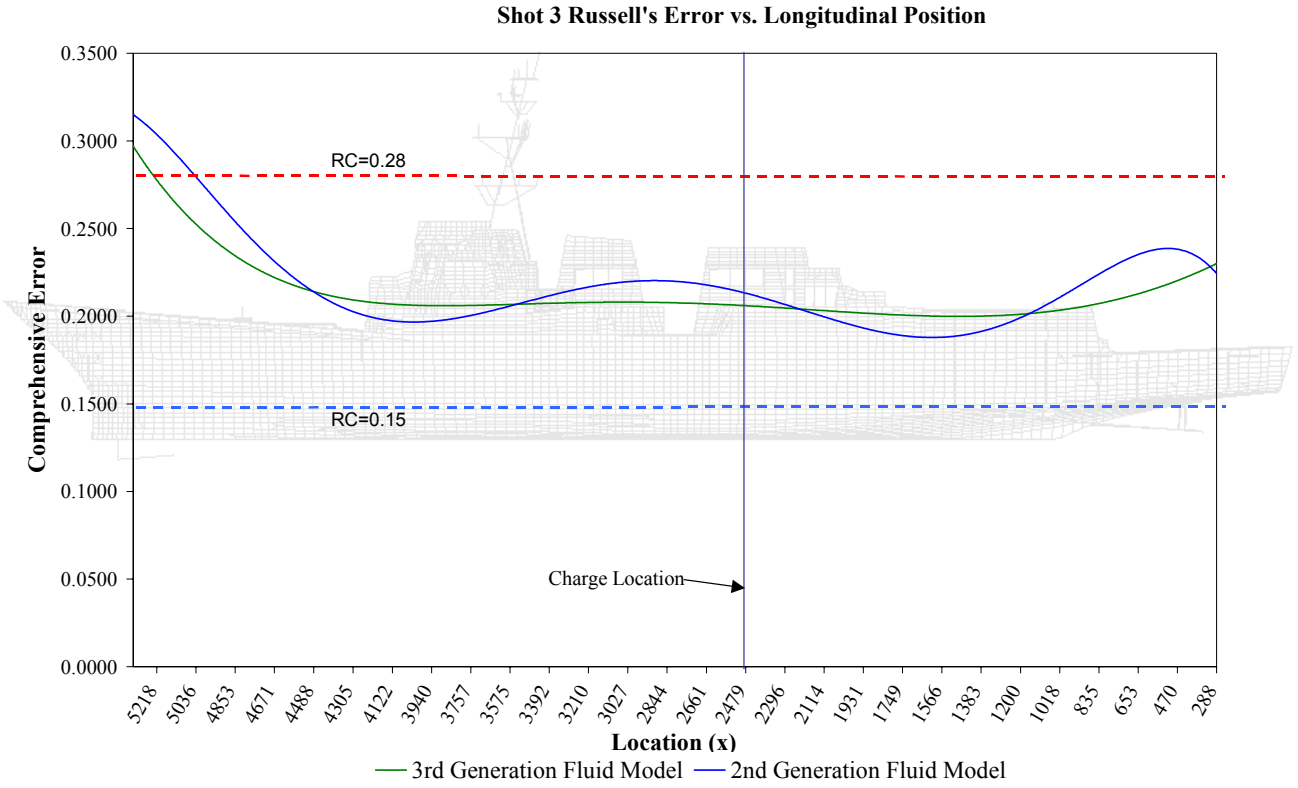

Figure 23. Comparison of 2nd and 3rd Generation Fluid Model Comprehensive Errors in Relation to Longitudianl Position along the Ship Model

Notable improvement in the error factor is shown in the regions around the sonar dome and the stern area, all areas where significant improvements were made to the mesh. However, the 2nd generation model had smaller errors in other regions of the ship. It indicates that other variables, such as data processing, sensor error, and environmental factors, have more of an effect on simulation error factors than small variations in the quality of the fluid model mesh. Figures 24 through 26 show three of the areas with the largest variations in error factors. With the exception of the sonar dome region, where the 3rd generation model does a better job of capturing the initial peak magnitude, the primary difference lies in the late time response.

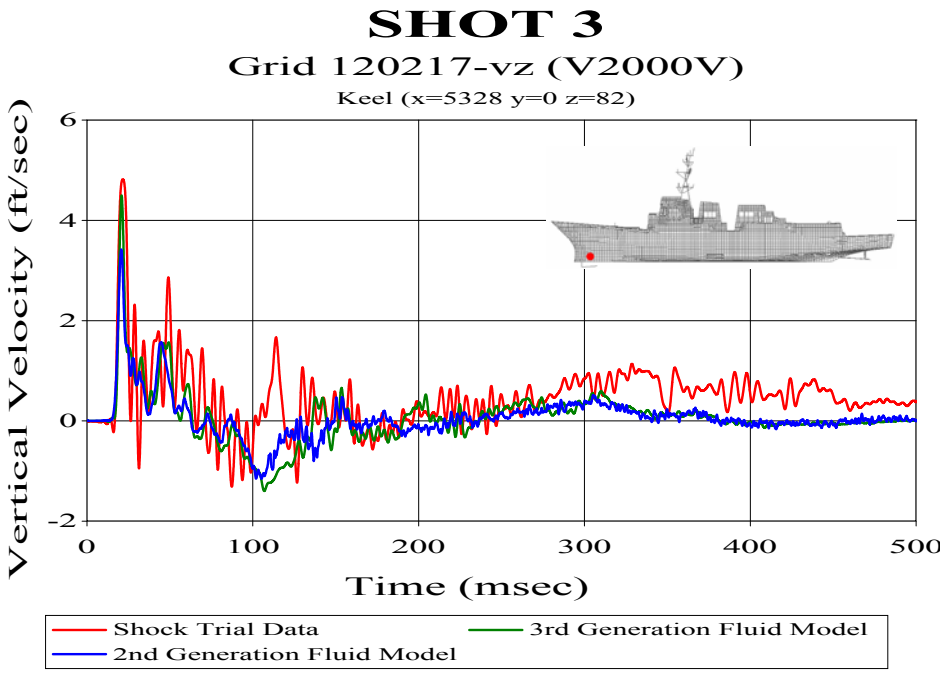

Figure 24. Sonar Dome Region Velocity Plot Comparison

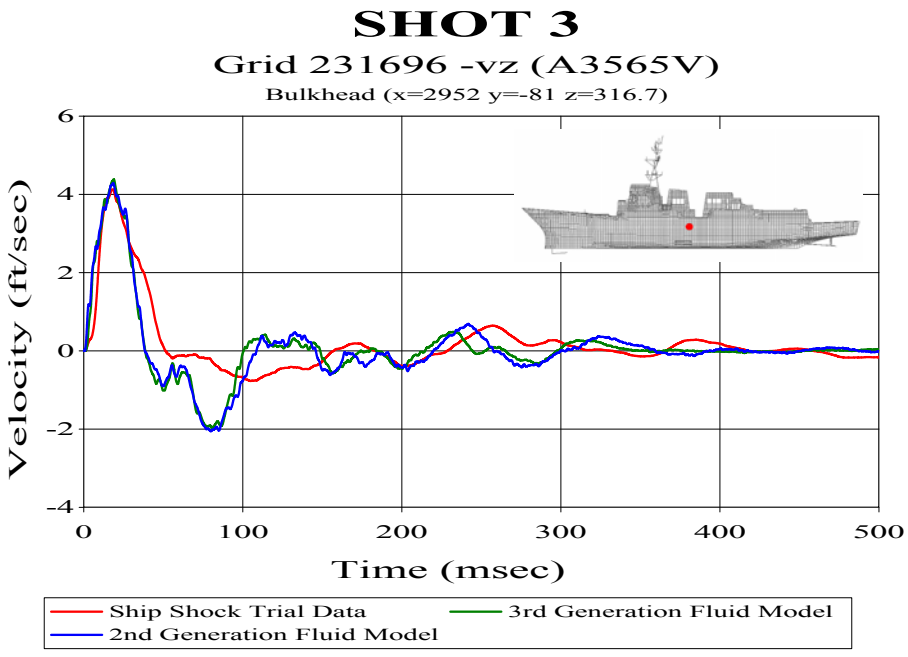

Figure 25. Midship Region Velocity Plot Comparison

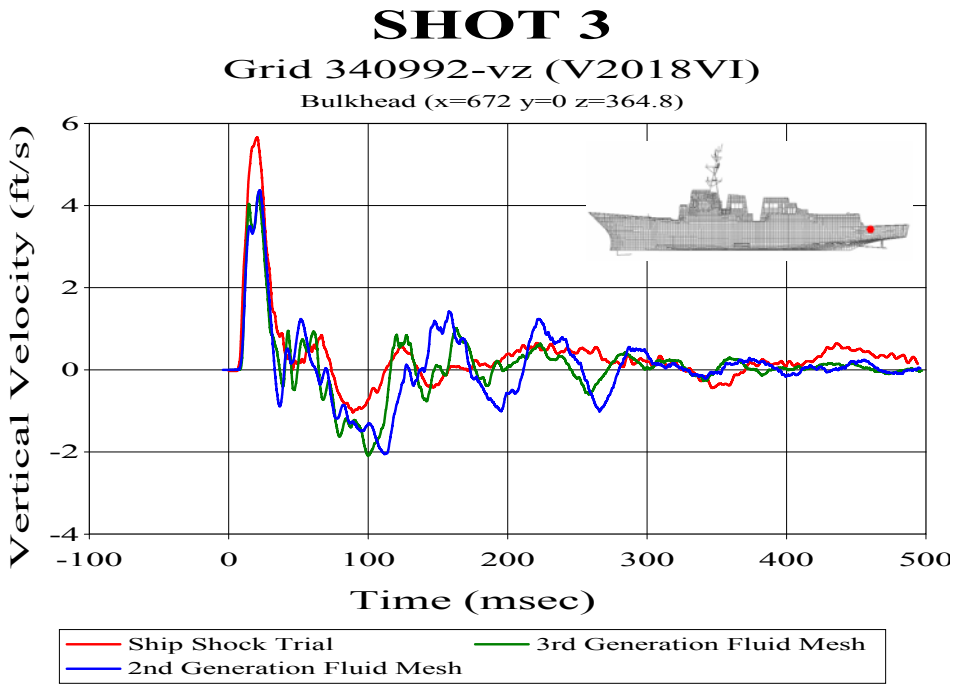

Figure 26. Stern Region Velocity Plot Comparison

Three fluid mesh FEM's of varying densities were modeled for Shot 3. All of the models maintained the same thickness of the inner two layers. The inner mesh and transitional mesh were varied from each having five to seven elements in the normal direction. The outer mesh was varied from having as few as 8 elements to as many as 23 elements in the normal direction. Table 5 lists a summary of the properties for each fluid model constructed for Shot 3. To avoid a sharp transition in the spacing of the elements in the coarse and medium fluid meshes, the outer mesh element spacing was graduated from smallest on the inner boundary to largest on the outer boundary. This was not required for the dense mesh. Table 5 lists the simulation run time. As shown, it took nearly five additional hours to run the dense model than the coarse model.

Table 5. Shot 3 Fluid Model Properties

Property	Coarse Mesh	Medium Mesh	Dense Mesh
Inner Mesh Elements	5	6	7
Inner Mesh Element Spacing (Ave.)	11.4 in	10.0 in	9.3 in
Transition Mesh Elements	5	6	7
Transition Mesh Element Spacing (Ave.)	13.4 in	11.6 in	10.1 in
Outer Mesh Elements	8	14	23
Outer Mesh Element Spacing (Ave.)	36 in	20 in	12 in
Fluid Nodes	150,607	197,429	250,181
DAA Elements	5048	5090	5132
Simulation Run Time	32.5 hrs	34.1 hrs	37.3 hrs

ERROR COMPARISON (SHOT 3)

The Russell's error factors are summarized in figures 27 through 29. The most significant change occurs between the dense and the medium mesh fluid model comparisons. The large number of negative magnitude error factors is indicative of the predicted response magnitude being lower than the measured response magnitude. The trend when increasing the density of the fluid mesh is that the errors tend to move primarily to the right and slightly downward. This indicates that the predicted response magnitude is increasing as the density of the mesh is increased. At the same time, though not as pronounced, the phase error is decreasing as the mesh density is increased.

.

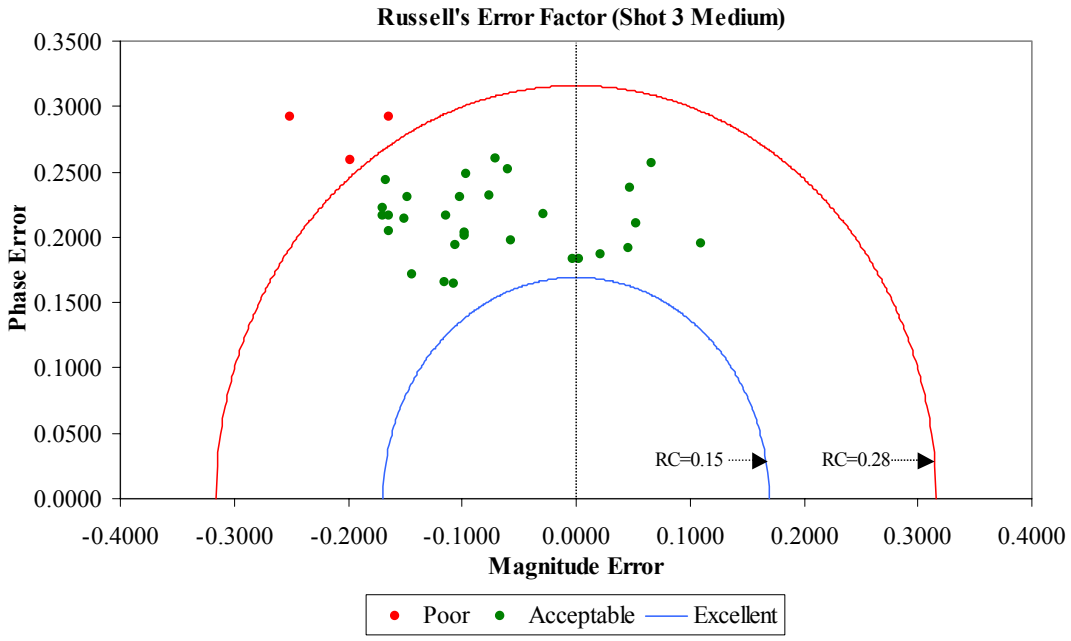

Figure 27. Russell's Error Factors for Coarse Mesh Fluid Model Comparison

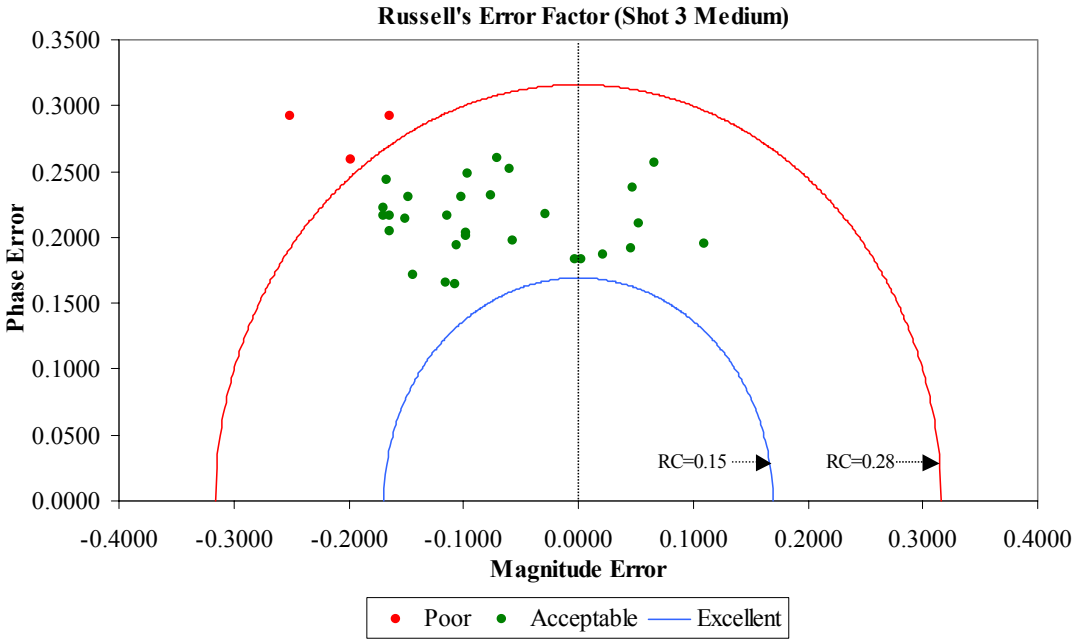

Figure 28. Russell's Error Factors for Medium Mesh Fluid Model Comparison

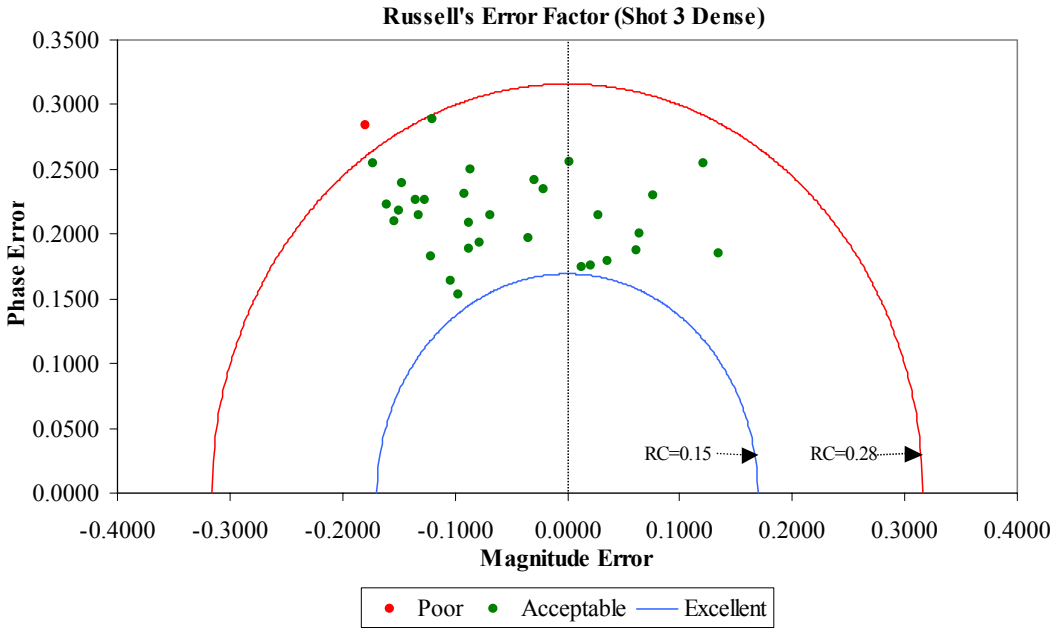

Figure 29. Russell's Error Factors for Dense Mesh Fluid Model Comparison

Figure 35 is a plot of the cumulative Russell's error factor trend for each fluid model as a function of the longitudinal position.

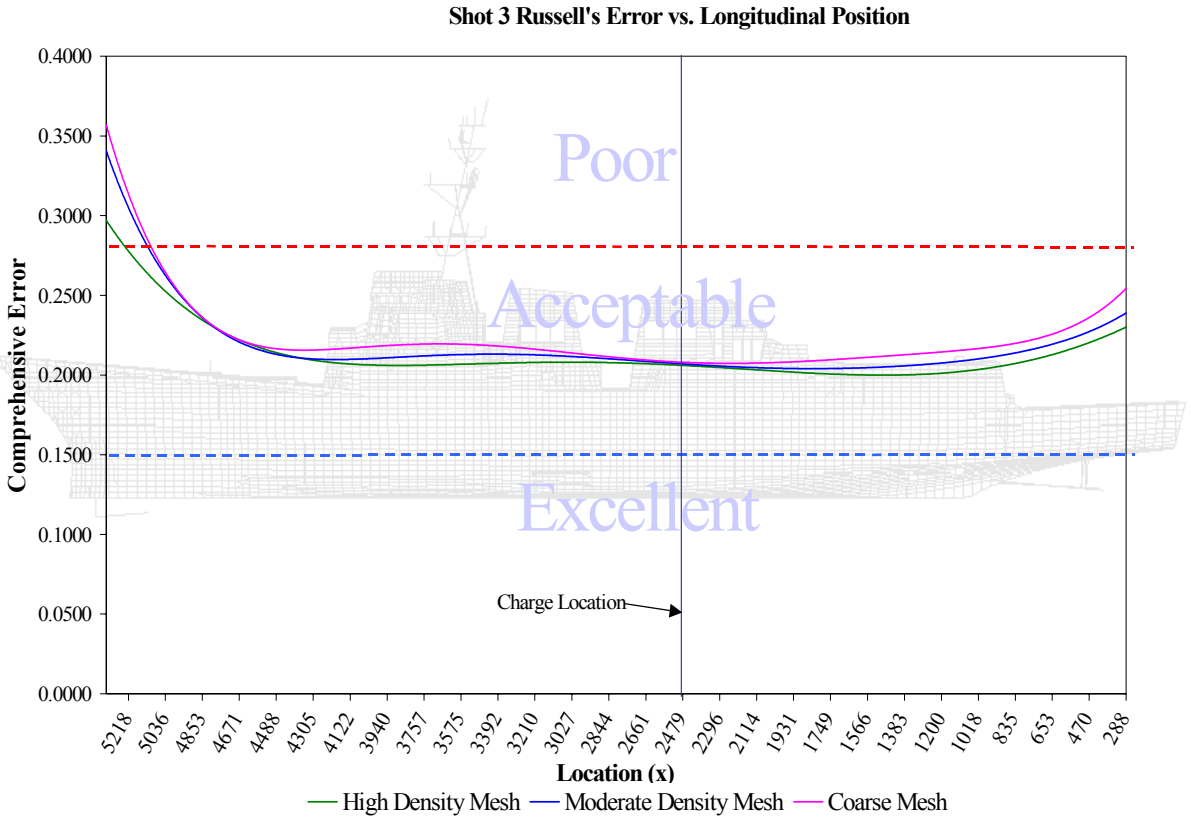

Figure 30. Russell's Comprehensive Error Trend along Longitudinal Position

For Shot 3, the shock wave initially impacts the structure at midships. Since the shock wave initiates at a node one element away from this point of impact, it propagates through very little of the fluid model before reaching the structure. The remainder of the structure, particularly the stern and bow sections, are not impacted until the shock wave has propagated through more of the fluid and structural model. The resulting error is reduced by increasing the normal direction mesh density, but not eliminated as shown in Figure 31. In terms of fluid mesh density comparison, it is apparent that the mesh density has the largest effect in these outer regions. Very little noticeable improvement is shown in the regions closest to the charge location.

It is useful to observe the velocity plots to help visualize how the predicted response varies as the fluid mesh density is increased. Figure 31 shows the predicted and measured 500 msec velocity response plots for keel sensor. This sensor is the forward most sensor, located above the sonar dome. This sensor resulted in the greatest comprehensive error in all three cases. From this plot it is evident that at least some of this error is due to the late time drift in the sensor. This drift was significant and could not be removed.

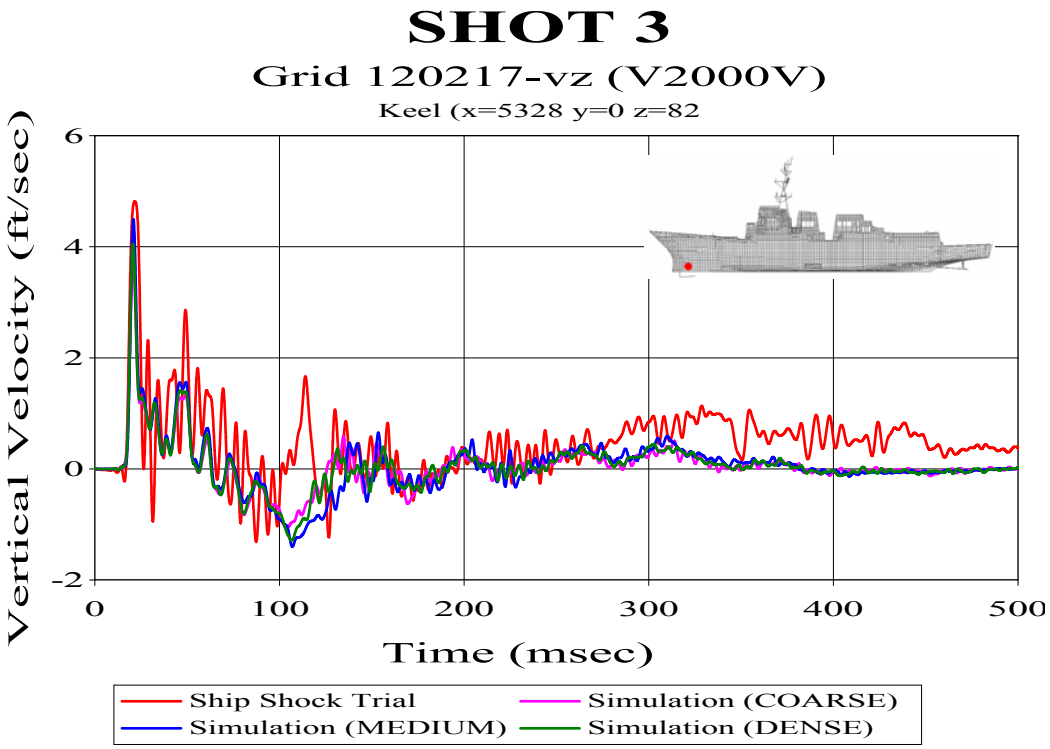

Figure 31. Velocity Response at Keel Sensor located above Sonar Dome

Figure 32 shows the velocity response plots for keel sensor. This sensor is significant as it is the closest sensor to the charge. This plot shows much better agreement between the predicted and measured response, having a comprehensive error factor of around 0.20 for all three fluid models. This plot also shows how the late time predicted response settles out similarly to the measured response. This is a measure of the quality of the ship system damping representation which appears to be very accurate in this case.

The third sensor shown is keel sensor shown in Figure 33. This sensor is one of the furthest aft sensors, located at frame 442. Due to excessive drift in the last portion of the sensor data only 350 msec of data was compared. Though better than sensor, this sensor shows how there are apparent transmission losses in the shock wave as it propagates outward through the fluid and structural model. Here the predicted late time response is in better agreement than the early time response. As in Figure 32, this is evidence of accurate system damping modeling.

Figure 34 shows bulkhead sensor. This sensor is bulkhead mounted on the starboard side, just forward of midships. Located higher in the structure than the four sensors shown above, this plot shows how the structure dampens the shock wave as it passes through. The response is more linear and settles down more rapidly than the keel response.

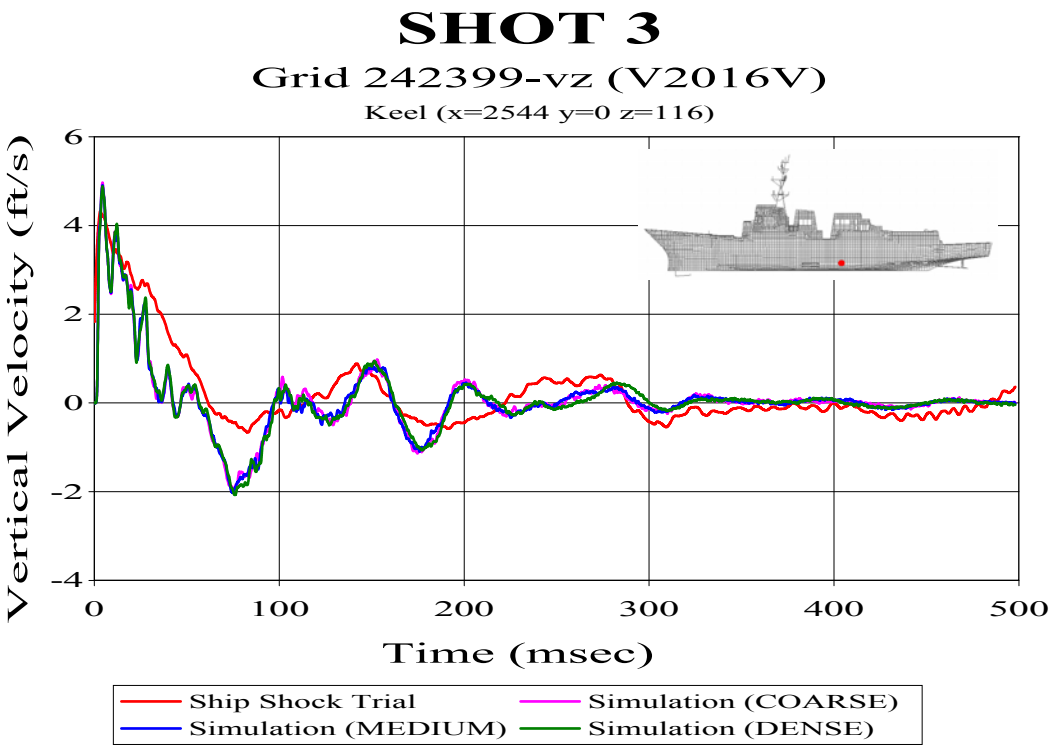

Figure 32. Velocity Response at Keel Sensor Close to the Charge

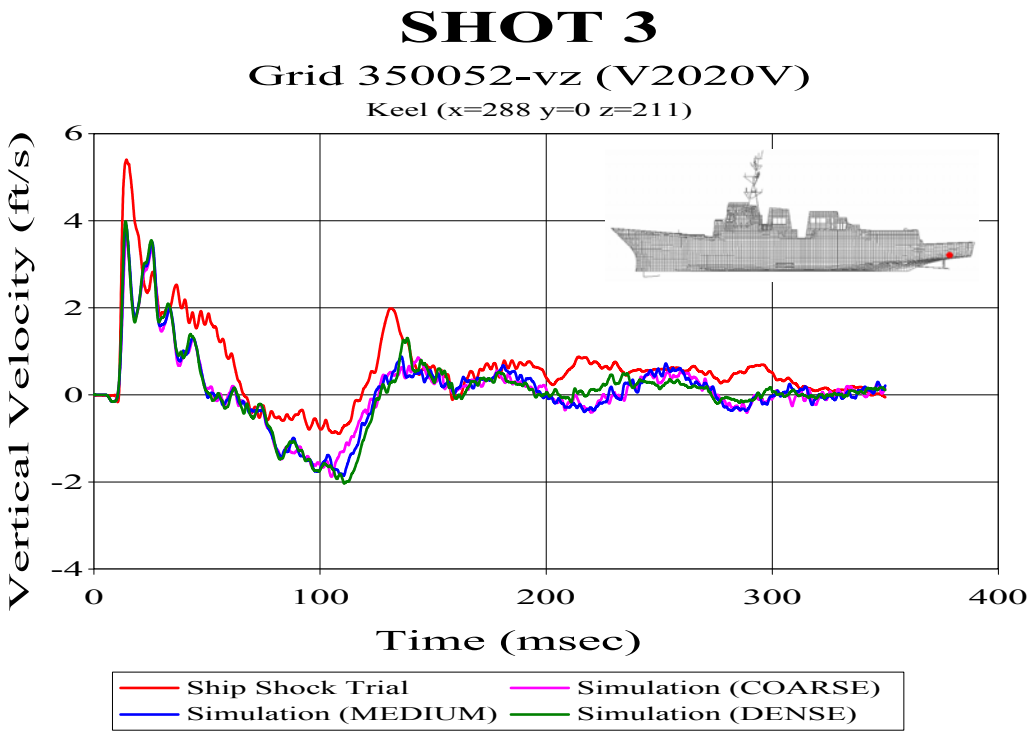

Figure 33. Velocity Response at Keel Sensor in Stern Area

This plot shows good agreement, both in phase and magnitude, between the measured and predicted velocity responses. The cumulative Russell's error factor for this comparison was 0.1838 for the dense fluid mesh, 0.1957 for the medium density fluid mesh, and 0.2013 for the coarse fluid mesh.

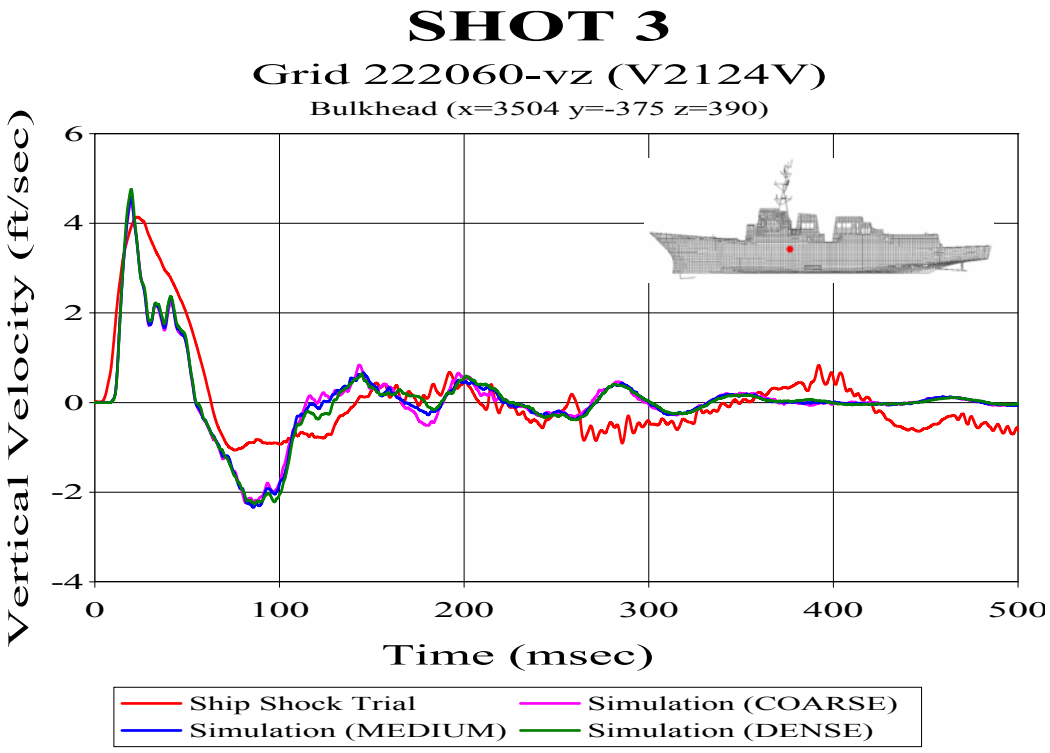

Figure 34. Velocity Response at Bulkhead Sensor

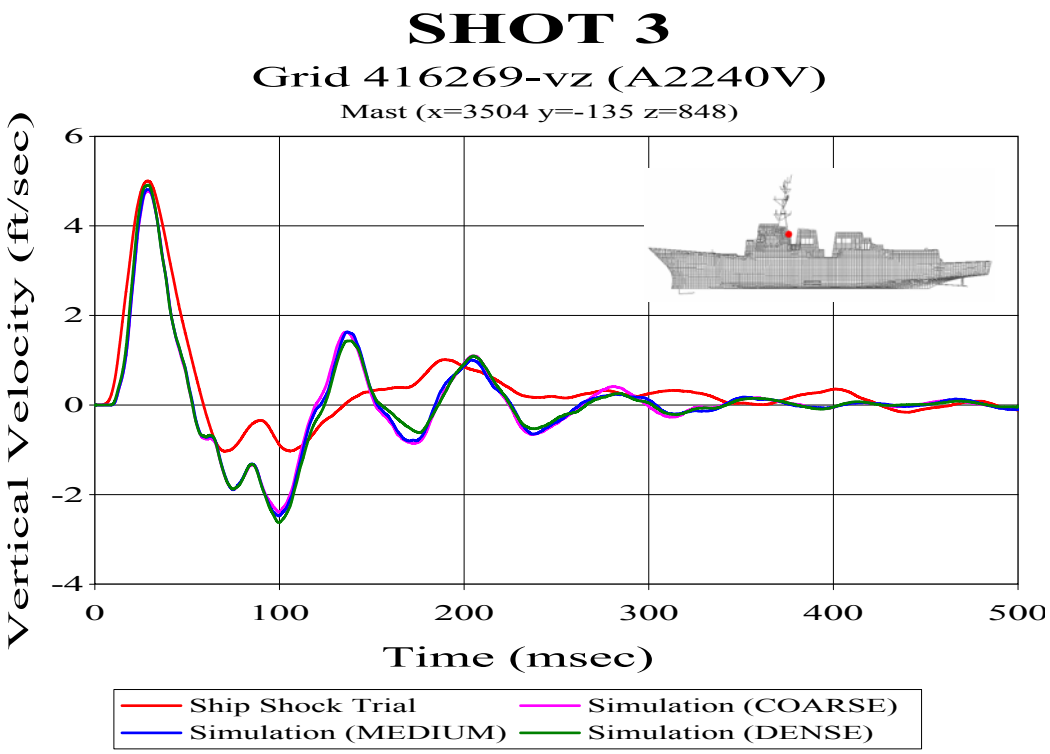

Figure 35. Velocity Response at Mast Leg Sensor

The velocity plot shown in Figure 35 above uses integrated acceleration data from accelerometer located on the starboard mast leg. This sensor had the best correlation between measured and predicted response of all sensors compared for this shot. The comprehensive error factor of the comparison using the dense mesh was 0.1552.

SHOT 1

The Shot 1, though the least severe, presented an interesting comparison due to its geometry. This shot was detonated outside of its intended box off the ship's port bow, its longitudinal position actually forward of the ship. Figure 36 shows the relative aspect of this shot to the ship.

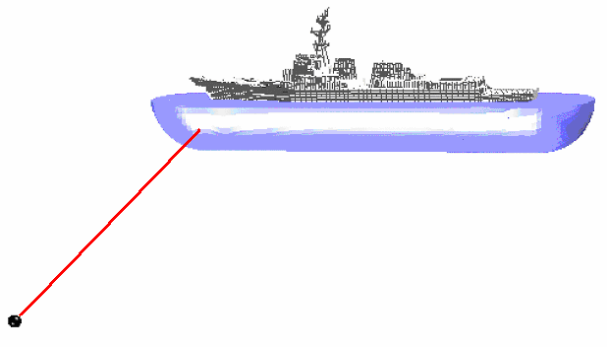

Figure 36. Shot 1 Geometry

Shot 1 was the furthest shot from the ship. As a result the fluid models were the largest cavitation depth models constructed, extending to a depth of 75 feet. For these models the number of normal fluid elements in the outer mesh ranged from 13 in the coarse mesh to 38 in the dense mesh. Table 6 summarizes the mesh properties of three of the fluid models constructed for the Shot 1.

Table 6. Shot 1 Fluid Model Mesh Properties

Property	Coarse Mesh	Medium Mesh	Dense Mesh
Inner Mesh Elements	5	6	7
Inner Mesh Element Spacing (Ave.)	11.4 in	10.0 in	9.3 in
Transition Mesh Elements	5	6	7
Transition Mesh Element Spacing (Ave.)	13.4 in	11.6 in	10.1 in
Outer Mesh Elements	14	24	38
Outer Mesh Element Spacing (Ave.)	36 in	20 in	12 in
Fluid Nodes	176,287	244,049	328,541
DAA Elements	5048	5090	5132
Simulation Run Time	34.75 hrs	40.48 hrs	47.33 hrs

The simulations of Shot 1 took considerably longer to run than Shot 3 due to the larger volume of the fluid mesh requiring more nodes. While all of the Shot 3 runs could be completed in a day and a half timeframe, the medium and dense mesh Shot 1 runs took nearly two days to process. While less than 5 hours separated the run times for all of the Shot 3 fluid meshes, there is over a 12 hour time difference between the coarse Shot 1 mesh and the dense

Shot 1 mesh run times. This time difference is indicative of how quickly the model grows in size when extending the depth of the fluid model.

ERROR COMPARISON (SHOT 1)

A summary of the Russell's error factors found for each model comparison are shown in Figures 37 through 39. Unlike the Shot 3 comparison error plots, there are no apparent trends in the Shot 1 comparisons. The plots suggest that there is a large variation in both phase and magnitude error as the error factors are very scattered in all three plots.

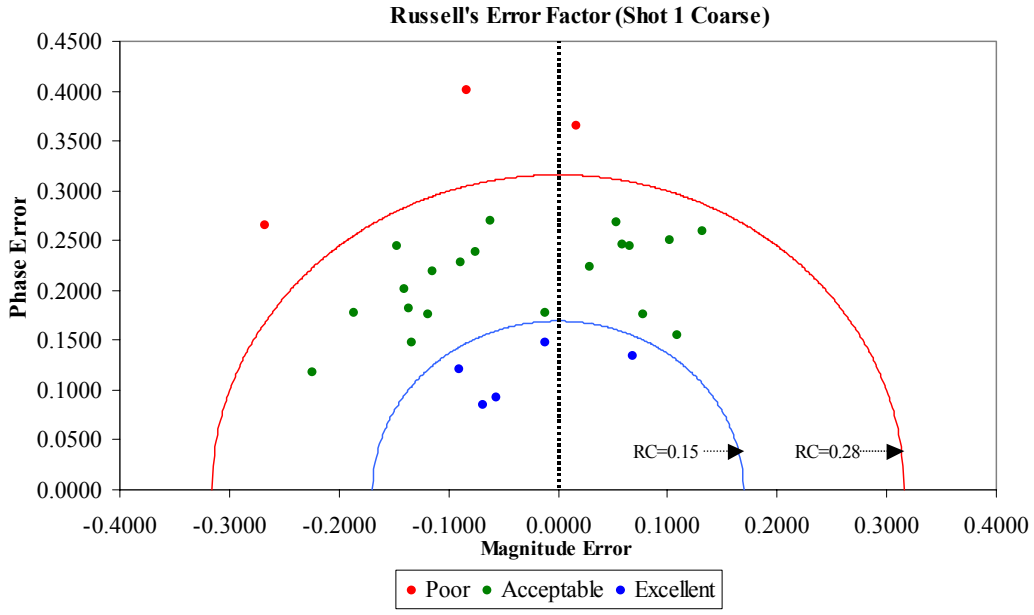

Figure 37. Russell's Error Factors for Course Mesh Fluid Model Comparison

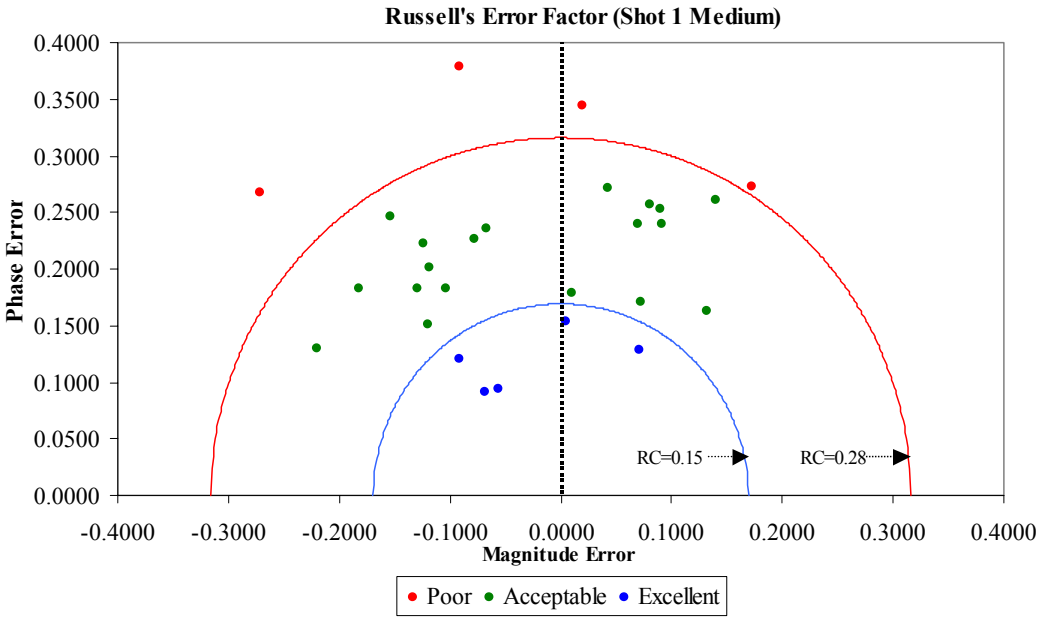

Figure 38. Russell's Error Factors for Medium Mesh Fluid Model Comparison

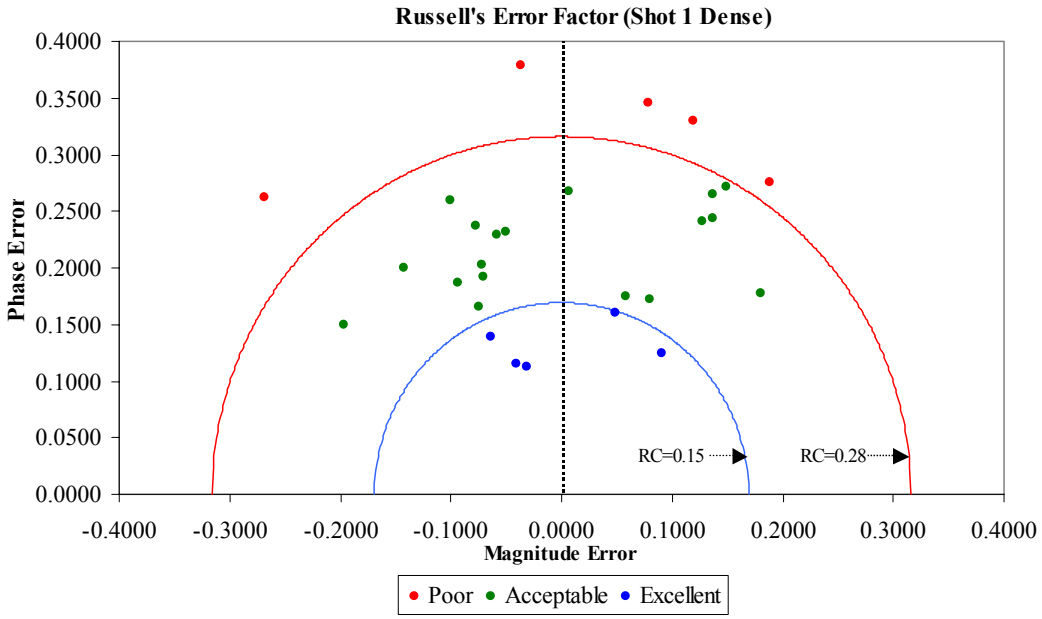

Figure 39. Russell's Error Factors for Dense Mesh Fluid Model Comparison

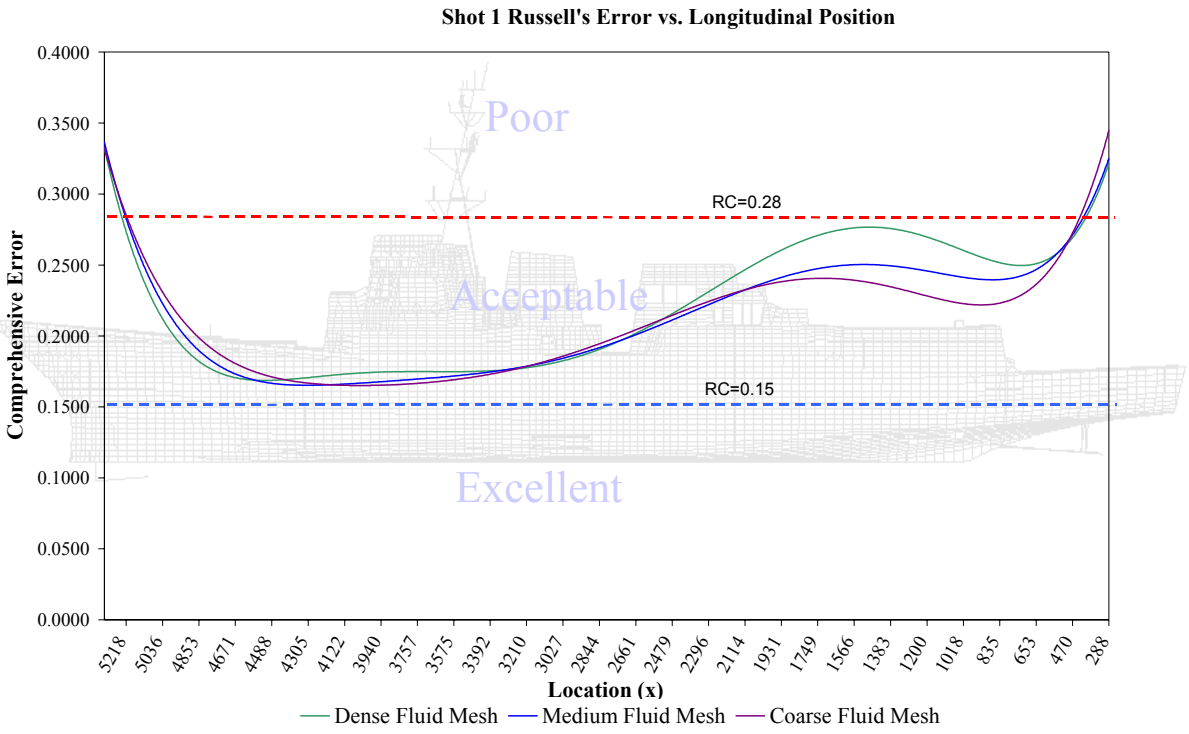

Figure 40. Russell's Comprehensive Error Trend along Longitudinal Position

Figure 40 shows the Russell's comprehensive error factor trend in relation to the longitudinal position on the ship for each fluid mesh. As is shown, all three meshes have poor correlation in the sonar dome region as was the case for Shot 3. For Shot 1 however, the sonar dome region was the closest region on the ship to the charge.

VELOCITY RESPONSES

To help visualize the Russell's error factor correlation discussed, three velocity plots are shown in Figures 41 through 43. Figure 41 shows bulkhead sensor, located forward of midships and above the waterline. This shows exceptional correlation in all three cases. The peak response is captured very well as is the recovery region immediately following this peak. The predicted response settles out faster than the measured response.

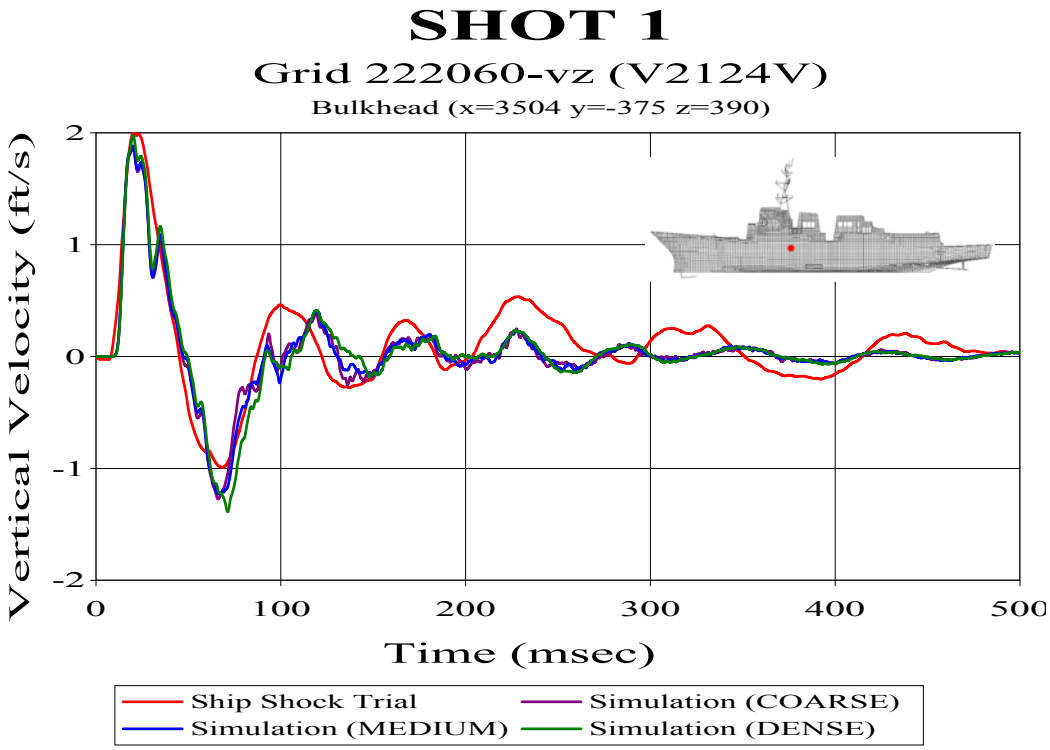

Figure 41. Velocity Response at Bulkhead Sensor

Shown in Figure 42, an accelerometer was located high in the structure on the starboard mast leg. Excellent phase and magnitude correlation is shown in this comparison. This excellent correlation shows. As with Shot 3, most of the comparisons made with accelerometer data showed significantly lower predictions errors than comparisons made with velocity meter data.

SHOT 2

The final shot compared is Shot 2. This shot was the only shot detonated on the starboard side of DDG 81. In this shot, the charge was located off the beam, slightly forward of where the Shot 3 charge was detonated on the port side and with a larger stand-off distance. Figure 43 shows the relative aspect of the Shot 2 charge to the ship.

Three 3rd generation models of varying density were constructed for the Shot 2 simulation. A summary of the fluid model properties is shown in Table 7.

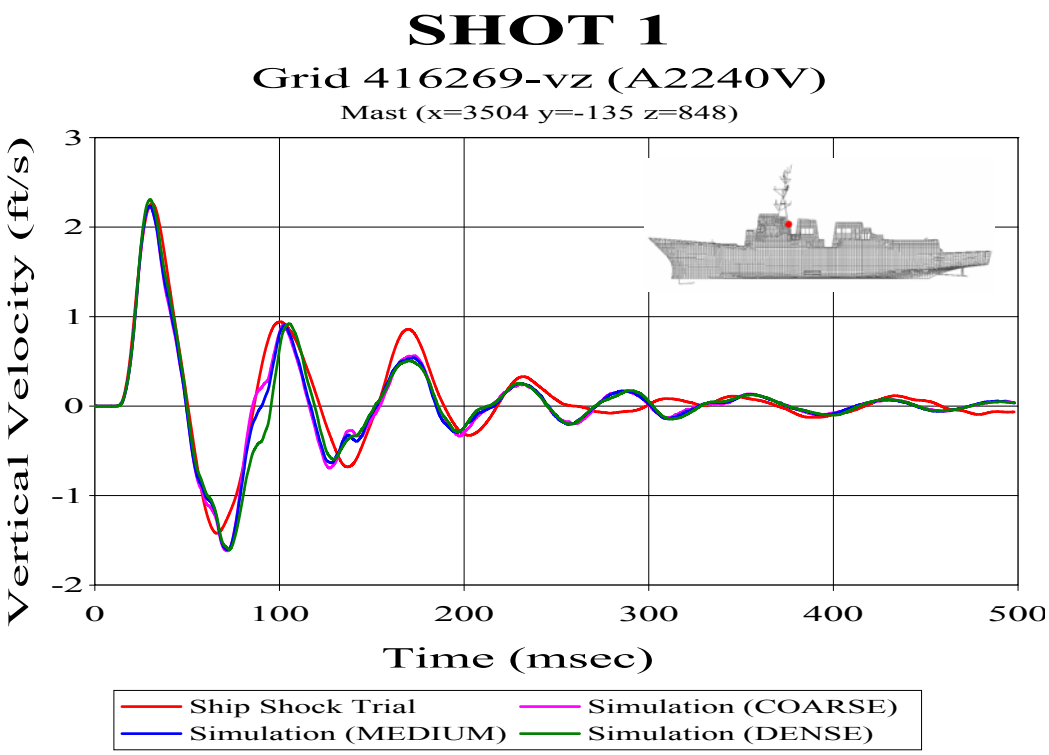

Figure 42. Velocity Response at Mast Leg Sensor

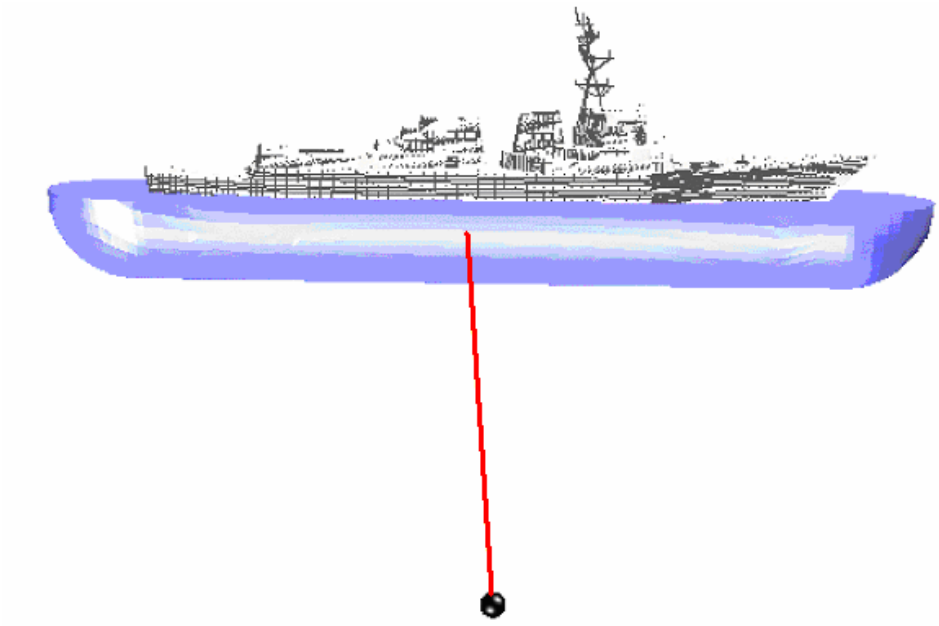

Figure 43. Shot 2 Geometry: Charge off Starboard Midships

Table 7. Shot 2 Fluid Model Properties

Property	Coarse Mesh	Medium Mesh	Dense Mesh
Inner Mesh Elements	5	6	7
Inner Mesh Element Spacing (Ave.)	11.4 in	10.0 in	9.3 in
Transition Mesh Elements	5	6	7
Transition Mesh Element Spacing (Ave.)	13.4 in	11.6 in	10.1 in
Outer Mesh Elements	10	20	32
Outer Mesh Element Spacing (Ave.)	36 in	20 in	12 in
Fluid Nodes	150,879	213,329	287,197
DAA Elements	5048	5090	5132
Simulation Run Time	31.5 hrs	37.2 hrs	42.8 hrs

ERROR COMPARISON (SHOT 2)

A summary of the Russell's error factors found in the comparison of all three meshes is shown in Figures 44 through 46.

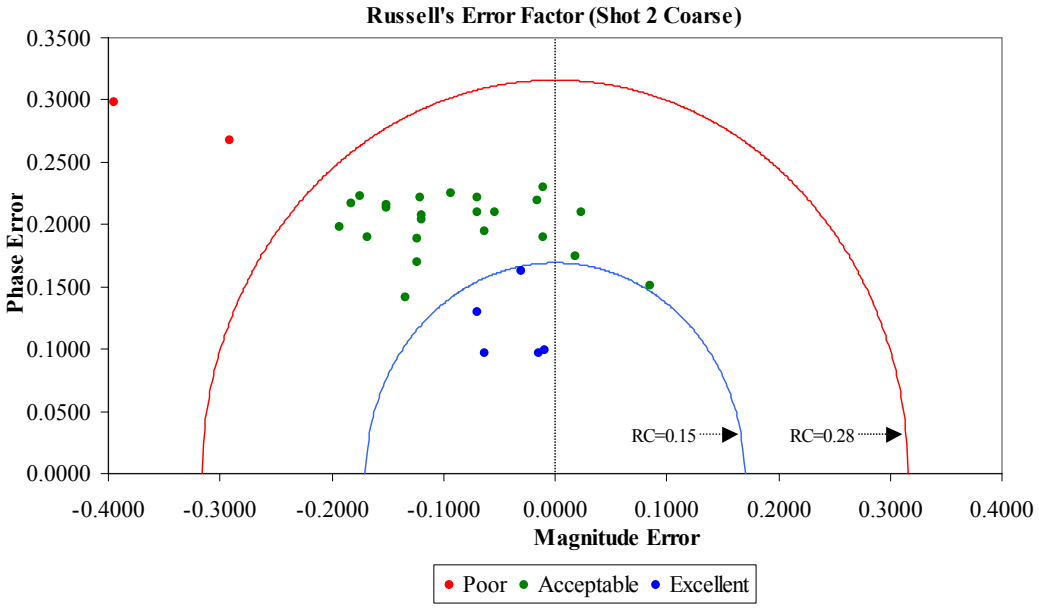

Figure 44. Russell's Error Factor for Coarse Mesh Fluid Model Comparison

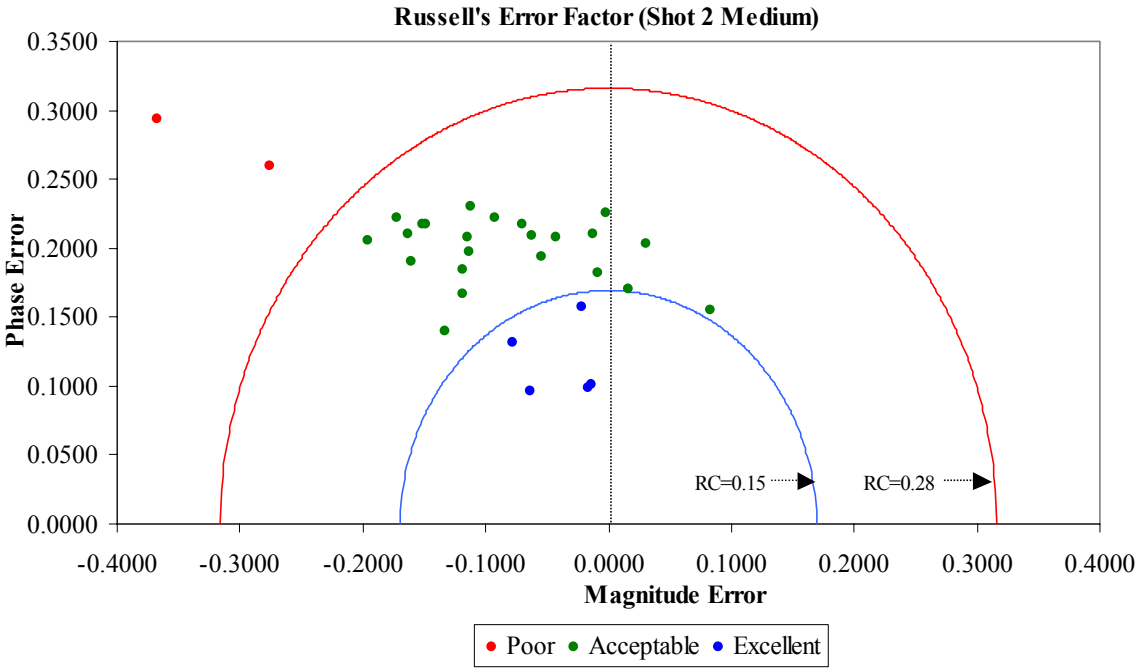

Figure 45. Russell's Error Factor for Medium Mesh Fluid Model Comparison

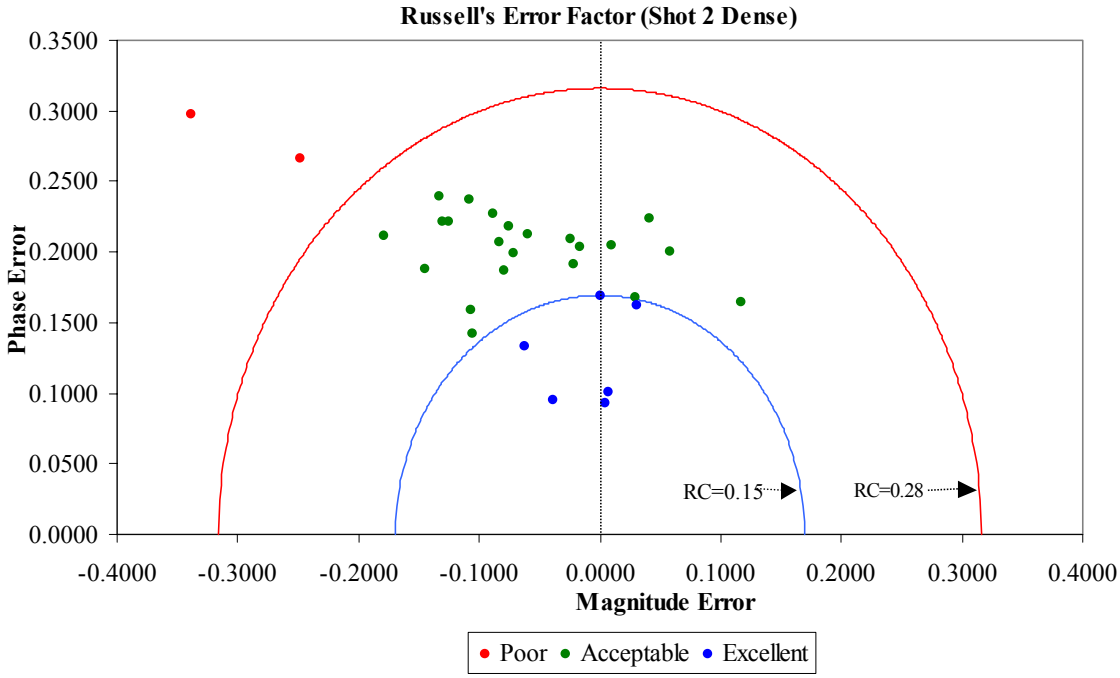

Figure 46. Russell's Error Factor for Dense Mesh Fluid Model Comparison

The trends in these comparisons are very similar to those observed in Shot 3. The dense mesh shows significant improvement in the overall error factors. This improvement is most significant in terms of the magnitude error. As in Shot 3, the general trend of the error factor plots is that the points move primarily to the right, indicative of a larger velocity magnitude response being predicted as the density of the fluid mesh is increased. The phase error remains fairly constant throughout.

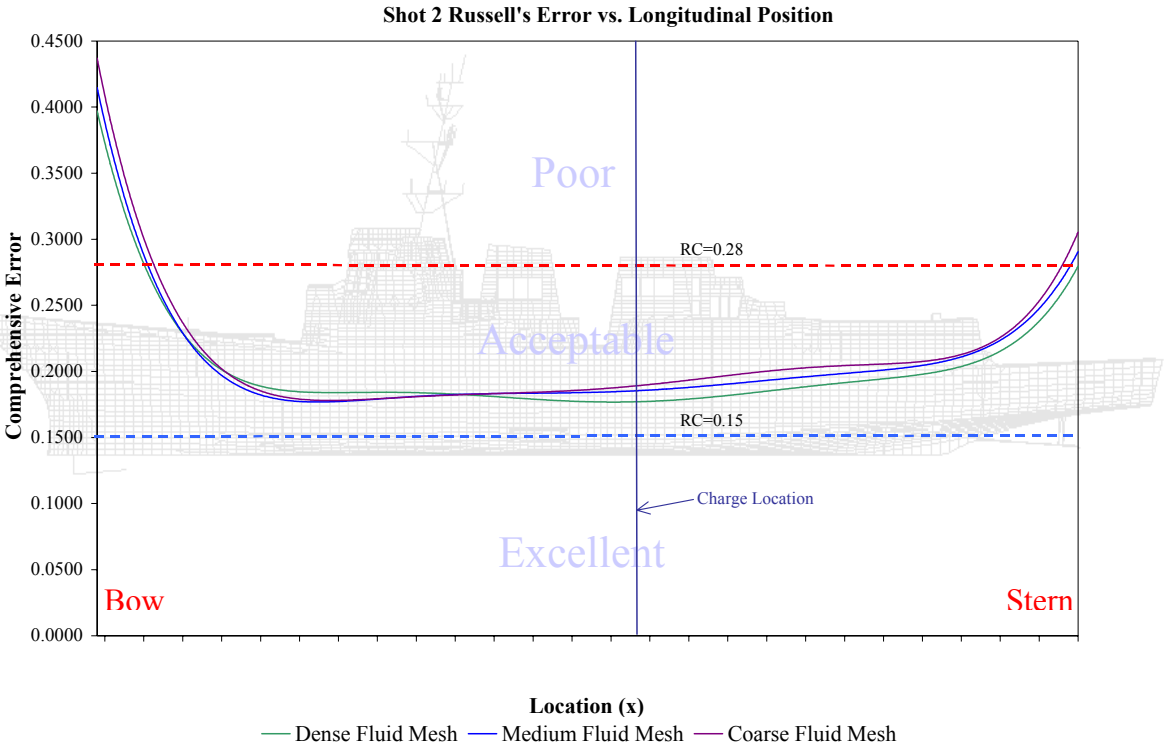

Figure 47. Russell's Comprehensive Error Trend along Longitudinal Position

Figure 47 shows the comprehensive error trends of each mesh comparison over the length of the ship. This trend plot shows that the most accurate predictions occur around the midship regions, while the least accurate predictions are at either end. The dense mesh shows a better prediction at these ends and in the aft section of the ship.

VELOCITY RESPONSES

Two velocity plots are shown in Figures 47 and 48. These plots show exceptional correlation in all cases. The peak response is captured very well as is the recovery region immediately following this peak.

Figure 47 shows bulkhead sensor. This sensor is located higher in the structure, making the prediction more dependent on the structural model and structural damping. Though showing signs of being slightly over damped, this comparison shows fairly good phase correlation. There is drift apparent in the late time measure response data that explains one reason why this sensor comparison had one of the highest comprehensive error factors of the Shot 2 sensors compared.

The last sensor comparison shown, mast sensor shown in Figure 48, had the best correlation of all of the comparisons for all three shots. The early time correlation between predicted and measured response was nearly perfect. Exceptional correlation was shown in the late time response correlation. Only a minor phase error exists and the model appears to be slightly over-damped. As in the previous two shots compared, significantly better correlation was observed when using measured data from accelerometers than with velocity meter data.

In conducting the fluid mesh density comparisons, several trends emerged which were prevalent in all three shot comparisons. In all cases, the predicted response correlation was better when comparing sensors mounted higher up in the structure.

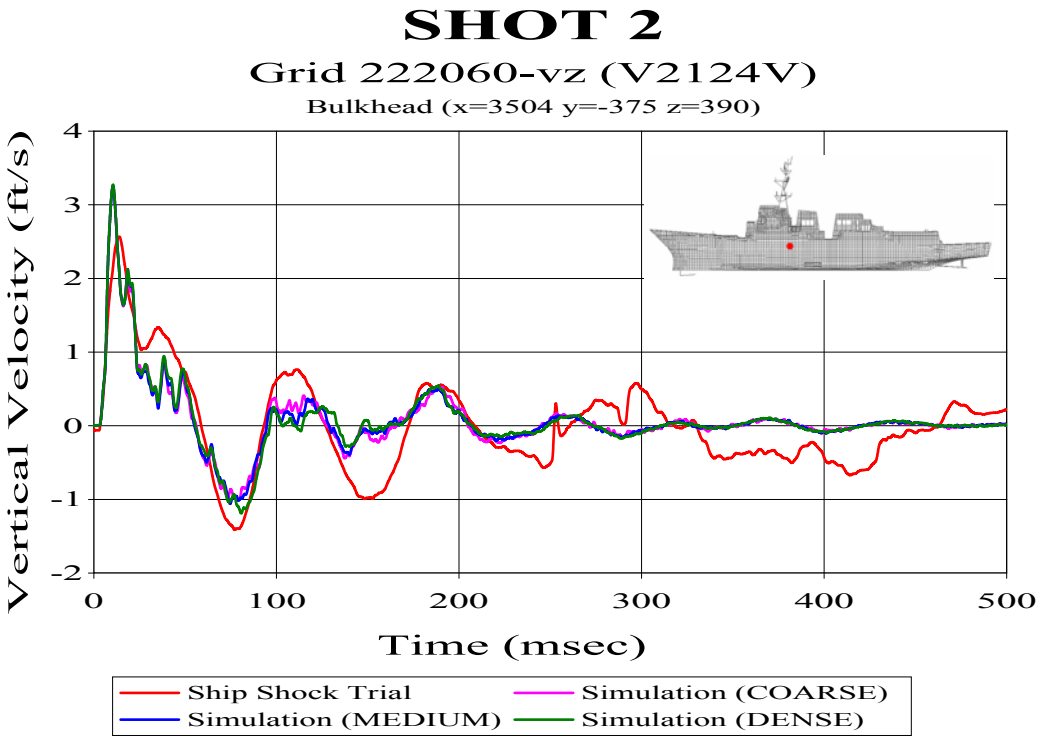

Figure 47. Velocity Response at Bulkhead Sensor

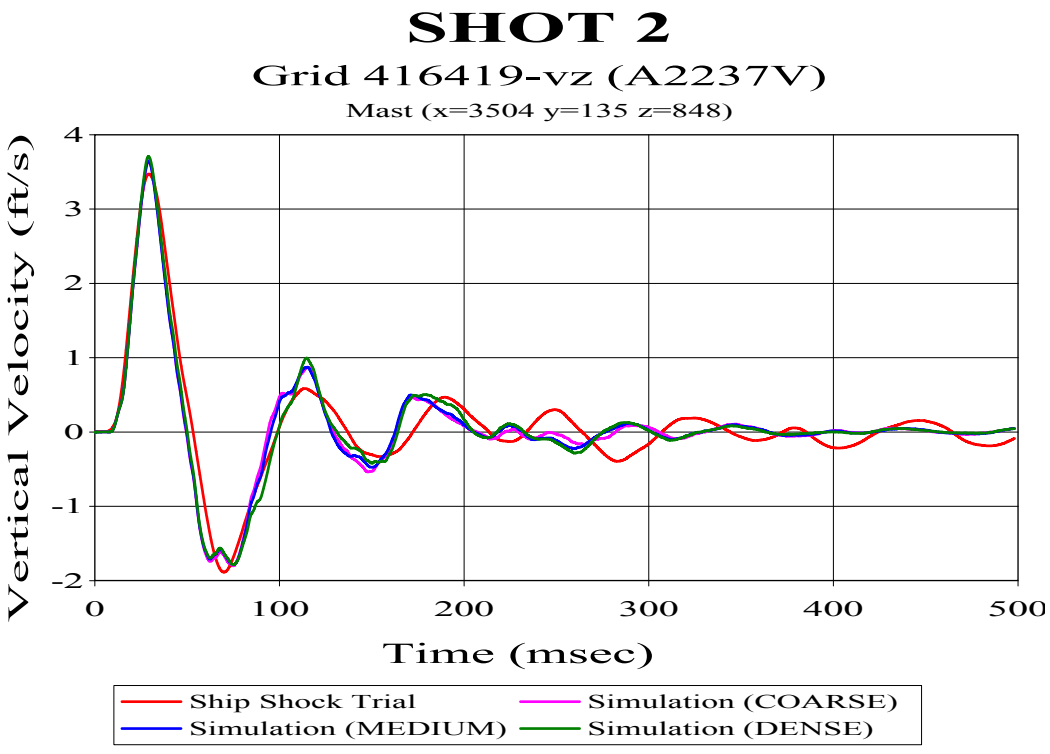

Figure 48. Velocity Response at Mast Leg Sensor

CONCLUSIONS

Creating a virtual underwater shock environment has proven to be a valid method of predicting the response of a surface ship to a variety of underwater explosions. Three separate underwater explosions were investigated in this paper, all of which produced acceptable vertical velocity response predictions overall. These underwater explosions originated from abeam the ship to off the bow, slightly forward of the ship. While the accuracy of these predictions falls off in regions of the ship furthest from the shot, the predictions in these regions still remain acceptable with only a few exceptions. The accuracy of the simulation predictions was shown to have little sensitivity to stand-off distance.

The depth of the fluid model had the largest impact on the accuracy of the predictions. A fluid model having a depth equal to the actual cavitation depth at the region closest to the charge resulted in the most accurate predictions. A fluid model having a depth equal to twice the cavitation depth yielded unacceptable predictions. This disparity appears to be due to the coarseness of fluid volume mesh away from the ship primarily resulting losses occurring in the incident pressure wave front. Fluid models having depths significantly less than the cavitation depth produced unacceptable results as well.

The fluid model mesh density was shown to have a significant effect on the simulation predictions. For shocks originating from abeam the ship, a fluid mesh having a higher mesh density was shown to provide substantially better predictions. For the shot off the bow, closer to being an end-on shot than a beam shot, the coarser mesh was shown to produce the most accurate predictions. It is theorized that this disparity is due to the tangential propagation of the shock wave and the resultant fluid particle velocities. In this direction, the coarser mesh has more preferable fluid element aspect ratios than the higher density meshes.

Small variations in the quality of the fluid mesh were shown to have measurable but minor effects on the accuracy of the overall simulation predictions. Although this study did not investigate the effects of gross variations in the quality of the mesh, minor improvements in the quality of the mesh were shown to result in overall improvement, but mixed results locally. Variables such as the size of the fluid mesh, the quality of the measured data, and environmental factors appear to outweigh any benefit gained by making small improvements in the quality of the mesh.

The correlation of the simulation predictions was found to be substantially better when being compared with accelerometer measured data than with velocity meter measured data. Substantial drift is apparent in nearly all of the velocity meter data. Data collected from accelerometer displayed significantly less drift even after being integrated. This suggests that a substantial amount of the calculated error may be due not to error in the simulation predictions, but in the measured data itself.

ACKNOWLEDGEMENTS

The authors are grateful for full sponsorship given by Naval Sea Systems Command, AEGIS Program Office(PMS 400D). The authors also extend their gratitude to CAPT David L. Lewis, CDR Jeffery S. Riedel and Mr. Constintine Constant for their continuous discussions and encouragement throughout the course of DDG 81 ship shock modeling and simulation. We would also like to thank Dr. R. Rainsberger for his support in fluid volume modeling using TrueGrid. Thanks are also due to Mr. T. Christian for his excellent job to make the computer always on-line and lastly to NPS Shock team for their tireless work.

LIST OF REFERENCES

1. NAVSEA 0908-LP-000-3010A, Shock Design Criteria for Surface Ships, October 1994.
2. Military Specification, MIL-S-901D, Shock Tests, High Impact Shipboard Machinery, Equipment and Systems, Requirements for, March 1989.
3. OPNAV Instruction 9072.2, “Shock Hardening of Surface Ships”, 12 January 1987

4. Mair, Hans U., Reese, Ronald, M., and Hartsough, Kurt, "Simulated Ship Shock Tests/Trials?", [www.dote.osd.mil/lfte/SSS.HTM]. April 2003.
5 Shin, Y.S. and Geers, T.L., "Response of Marine Structures Subjected to Underwater Explosions," *International Short Course Notes*, Shock and Vibration Research.
6. XYZ Scientific Applications, Inc., *TrueGrid User Manual Version 2.4*, Livermore, CA 2002.
7. Livermore Software Technology Corporation, *LS-DYNA Keyword User's Manual*, Version 960, LSTC, Livermore, CA, March, 2001.
8. DeRuntz, Jr., J.A., The Underwater Shock Analysis (USA) Manual, Unique Software Applications, Colorado Springs, CO, May 1996.
9. Gibbs and Cox, Inc., "DDG-81 Flight IIA Shock Simulation", Presentation at the Naval Postgraduate School, August 2002.
10. Shin, Y.S., and Santiago, L.D., "Surface Ship Shock Modeling and Simulation: 2D Analysis," Journal of Shock and Vibration, Vol. 5, No. 2, 1998, John Wiley & Sons, Inc.
11. Shin, Y.S. and Park, S.Y., "Ship Shock Trial Simulation of USS John Paul Jones (DDG 53) Using LS-DYNA/USA: Three Dimensional Analysis", *70th Shock and Vibration Symposium Proceedings*, Vol. I, November 1999.
12. Malone, P. E. and Shin, Y. S., "Sensitivity Analysis of Coupled Fluid Volume to Ship Shock Simulation," *Proceedings of 71st Shock And Vibration Symposium,* Crystal City VA, 6-9 Nov., 2000.
13. Shin, Y.S., "Ship Shock Modeling and Simulation for Far-Field Underwater Explosion," To be appeared in *Computer & Structure Journal*, Spring 2004.
14. MacNeal-Schwendler Corporation, "MSC/NASTRAN Quick Reference Guide," Version 69, Los Angeles, CA, 1996.
15. Smith, J.W., Vibration of Structures: Applications in Civil Engineering Design, 338p., Chapman and Hall, London, 1988.
16. Shin, Y.S. and Ham, I.B. "Damping Modeling Strategy for Naval Ship System", *Report NPS-ME-03-003, Naval Postgraduate School,* September, 2003; Also Proceedings of Shock and Vibration Symposium, San Diego CA, 27-31 October, 2003.
17. TEAM Engineering Ltd, "FEMAP: Real FEA Made Easy", [http://www.femap.co.uk]. May 2003.
18. DeRuntz, Jr., J.A. "The Underwater Shock Analysis Code and Its Applications", *60th Shock and Vibration Symposium*, Vol. I, pp. 89-107, November, 1989.
19. Geers, T.L., "Doubly Asymptotic Approximations for Transient Motions of Submerged Structures", The *Journal of the Acoustical Society of America*, Vol. 64, pp 1500-1508, 1978.
20. DeRuntz, Jr, J.A. "Application of the USA Code to Underwater Shock Problems", *72nd Shock and Vibration Symposium,* November, 2001.
21. Wood, S. L. and Shin, "Caviation Effects to Ship-like-Box Structure for Underwater Explosion," Presented at *69th Shock and Vibration Symposium*, Oct. 12-16, 1998, Minneapolis/St. Paul, MN.
22. Deruntz, Jr.,J.A. and Shin, Y.S., "USA/LS-DYNA3D Software Training Course", Naval Postgraduate School, Monterey, CA, June 1996.
23. Ceetron ASA, "Glview Pro Installation Guide & Tutorial: Glview Pro 6.3", Trondheim, Norway, 2001.
24. Thomas, P.D. and Middlecoff, J.F., "Direct Control of the Grid Point Distribution in Meshes Generated by Elliptic Equations*", AIAA Journal*, Vol. 18, June, 1980.
25. Bouche, R.R., *Calibration of Shock and Vibration Measuring Transducers*, pp. 22-115, Naval Research Laboratory, 1979.
26. Russel, D.D., "Error Measures for Comparing Transient Data: Part I: Development of a Comprehensive Error Measure", *68th Shock and Vibration Symposium Proceedings*, Vol. I, November 1997.
27. Russell, D.D., "DDG53 Shock Trial Simulation Acceptance Criteria", *69th Shock and Vibration Symposium*, October 1998.
28. Russel, D.D., "Error Measures for Comparing Transient Data: Part II: Error Measure Case Study", *68th Shock and Vibration Symposium Proceedings*, Vol. I, November 1997.
29. Hart, D.T., "Ship Shock Trial Simulation of USS Winston S. Churchill (DDG-81): Surrounding Fluid Effect", Master's Thesis, Naval Postgraduate School, Monterey, CA, 2003.